FINITE RANGE EFFECTS IN (d,p) STRIPPING REACTIONS USING THE WBP MODEL

by

John Morgan CoVan

A Dissertation Submitted to the Faculty of the

DEPARTMENT OF PHYSICS

In Partial Fulfillment of the Requirements
For the Degree of

DOCTOR OF PHILOSOPHY

In the Graduate College

THE UNIVERSITY OF ARIZONA

1 9 7 3

THE UNIVERSITY OF ARIZONA

GRADUATE COLLEGE

I hereby recommend that this dissertation prepared under my direction by John Morgan CoVan

entitled FINITE RANGE EFFECTS IN (d,p) STRIPPING REACTIONS USING THE WBP MODEL

be accepted as fulfilling the dissertation requirement of the degree of Doctor of Philosophy

C. A. Barnes — 3.20.73
Dissertation Director — Date

Sigurd Kahn — 3.28.73
Co-Dissertation Director — Date

After inspection of the final copy of the dissertation, the following members of the Final Examination Committee concur in its approval and recommend its acceptance:*

Donald R. Huffman — 4-2-73

R C Oni Intyre — 4-3-73

R. M. Kalbach — 4.5.73

Michael Scadron — 4-6-73

*This approval and acceptance is contingent on the candidate's adequate performance and defense of this dissertation at the final oral examination. The inclusion of this sheet bound into the library copy of the dissertation is evidence of satisfactory performance at the final examination.

STATEMENT BY AUTHOR

This dissertation has been submitted in partial fulfillment of requirements for an advanced degree at The University of Arizona and is deposited in the University Library to be made available to borrowers under rules of the Library.

Brief quotations from this dissertation are allowable without special permission, provided that accurate acknowledgment of source is made. Requests for permission for extended quotation from or reproduction of this manuscript in whole or in part may be granted by the head of the major department or the Dean of the Graduate College when in his judgment the proposed use of the material is in the interests of scholarship. In all other instances, however, permission must be obtained from the author.

SIGNED: John M. Glan

ACKNOWLEDGMENTS

I would like to thank my adviser, Professor C.A. Pearson, for his many hours of guidance and encouragement which added much to the success of my research. I am deeply indebted to Dr. F.P. Gibson for many enlightening discussions.

This work was supported in part by the National Science Foundation. The major portion of the computations were performed in the Rust Research Center at the University of Alabama in Birmingham. Additional computations were performed at Redstone Arsenal and Oak Ridge National Laboratory.

TABLE OF CONTENTS

TABLE OF CONTENTS--Continued

LIST OF ILLUSTRATIONS

LIST OF TABLES

ABSTRACT

An approximate method is developed for including effects of a finite range neutron-proton potential V_{np} in calculations for the Weakly Bound Projectile (WBP) model for stripping reactions. The method is similar to the approximate finite range calculations for the distorted wave Born approximation in its use of an expansion method involving the short range of V_{np}. However the method avoids the difficulties associated with these previous applications. For an appropriate choice of V_{np} the expansion in the WBP amplitude is shown to converge, so that the accuracy of the method is determined by the accuracy of the numerical procedures used.

The application of the method requires a simple modification of previous zero range calculations and does not significantly increase the time required for computation.

Several central potential forms (square well, Gaussian and Yukawa) consistent with low energy two-nucleon scattering are considered for the neutron-proton interaction. Approximate finite range WBP model calculations are reported for the square well and Gaussian forms and the results are shown to be independent of the potential shape. Calculations are also reported which check the effect of truncating the finite range expansion.

Qualitative and quantitative effects were observed by comparing zero range and finite range calculations for (d,p) reactions on the target nuclei ^{16}O, ^{40}Ca and ^{90}Zr for values of ℓ_n ranging from 0 to 3.

Qualitative changes of the polarization and vector analyzing power were small and no regular trends were apparent. The differential cross section tended to be reduced slightly at the stripping peak and at back angles. The most important quantitative effect shown is on the spectroscopic factor which is extracted from the calculated differential cross section. Spectroscopic factors extracted with zero range and finite range codes are compared. Corrections to the spectroscopic factors for light nuclei can be as large as +25%.

CHAPTER 1

INTRODUCTION

For more than twenty years measurements on the outgoing particle in deuteron stripping reactions have been used to obtain information concerning the structure of the residual nucleus[1-7]. From the early measurements using unpolarized deuteron beams, it was found that the angular distribution for the outgoing particle often can be used to determine the parity of the residual nucleus. The angular dependence of the polarization P_y can also be used to determine the total angular momentum j for this nucleus[8-14]. In addition, careful measurement of the magnitude of the differential cross section $d\sigma/d\Omega$ can be used to extract the spectroscopic factor S associated with the single particle structure of the residual nucleus[15-24].

The development of polarized ion sources[25-31] has increased the potential of deuteron stripping and pickup reactions for providing information concerning nuclear structure. Measurements of vector analyzing power P_D can reveal the value of j for certain states in an unambiguous way[32,33]. Such measurements can also help refine models used for interpreting the data and hence lead to more precise spectroscopic factors.

Improved calculations concerning the microscopic structure of low-lying states have recently been reported for many nuclei[34-40]. These advances in nuclear structure calculations have been accompanied by

experiments in which detailed angular distributions including absolute magnitudes have been measured for (d,p) reactions which lead to an extended sequence of final states in the residual nucleus[41-43]). To take full advantage of the polarized sources and to extract from the (d,p) reaction measurements information which is accurate and reliable enough to test the nuclear structure calculations, some effort must be spent on improving the models of the reaction mechanism.

Since the discovery of stripping reactions and their initial interpretation by Butler[1]) there has been considerable development of the reaction models. The initial Butler model was a three-body model in which the neutron and proton wave functions are represented by plane waves with a spherical hole in the vicinity of the nucleus. Because the distortion of the neutron and proton wave functions by the interaction with the target nucleus was represented so crudely with no spin dependence, the Butler model consistently overestimated the cross section by one or two orders of magnitude and predicted the outgoing nucleon to be unpolarized.

The emergence of the zero range distorted wave Born approximation (DWBA) accompanied development of fast digital computers in the late 1950's and early 1960's[44-49]). By taking more realistic account of the interactions with the target nucleus, this model was able to predict better agreement with the shape and magnitude of measured differential cross sections. However, in order to make use of realistic interactions with the target nucleus, the DWBA abandons the three-body mechanism in which the neutron and proton have semi-independent motion, treating the deuteron as one would a tightly bound particle - the internal motion of

which is left undisturbed by its passage through the nucleus. Thus stretching and orientation of the deuteron by the nuclear field were ignored. (Some efforts have been made to correct this recently[50,51].)

Because of the weak binding and large size of the deuteron, in the situation shown in Fig. 1, the potential energy difference between neutron and proton is much greater than the deuteron binding energy. One might therefore expect effects neglected in the DWBA to be significant.

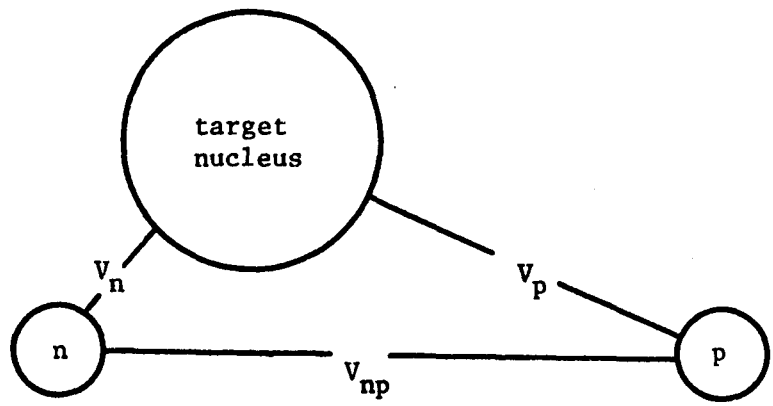

Fig. 1. Two-body Potentials Used in the WBP Model

The Weakly Bound Projectile (WBP) model was developed to take proper account of the weak binding of the deuteron[52-55]. This model revived the three-body description of the original Butler model. The interactions which are involved in the stripping mechanism being the neutron-proton interaction V_{np}, and the separate interactions V_n and V_p of the neutron and proton with the target nucleus. The initial calculations with a zero range form of the WBP model showed good agreement with

the angle dependence of measured differential cross sections, polarization and vector analyzing power[56-59]).

Various refinements have been made to the original WBP model calculations. The contributions from the D-state component of the deuteron internal wave function[60]), corrections arising from non-locality of the nucleon-nucleus optical potentials[61]) and a realistic (Hamada-Johnston) deuteron wave function[62]) have been taken into account.

In the DWBA calculations the effects of the deuteron D-state[63,64]) and non-locality[65-76]) have also been considered. However in addition, various attempts have been made to include in the DWBA calculations the corrections which arise from the finite range of the neutron-proton interaction V_{np}[77-84]). While these attempts have met some difficulties - the "exact" calculations proving cumbersome[79,80]), and the "approximate" calculations proving inaccurate[81,82]) - they have shown that finite range corrections can make significant changes to the magnitude of the predicted cross sections and hence to the spectroscopic factors extracted therefrom. No corresponding calculations of polarization and vector analyzing power using the DWBA have been reported.

The nature of the finite range corrections to the DWBA calculations has made it necessary to examine the corresponding effects in the WBP model calculations. Not only must the influence of these corrections on the magnitude of spectroscopic factors be determined, but also their influence on the qualitative behavior of the calculated polarization and vector analyzing power from which the j values are found.

In this dissertation a convenient method for including finite range corrections in WBP model calculations is developed. The method is not as cumbersome and time-consuming to calculate as "exact" finite range calculations in the DWBA. It is similar to the approximate finite range calculations for the DWBA (see approximations referred to as "LEA"[79,82]) and "EMA"[82-84]) in Appendix B) in its use of an expansion involving the short range of V_{np}. However, the method is more accurate than the LEA and EMA. For appropriate potentials V_{np} the method can be shown to converge within the accuracy of the numerical procedures used. The application of the method requires a simple modification of the zero range computer code and does not significantly increase the time for computation.

In Chapter 2 we review the basic assumptions of the WBP model to put the finite range and zero range approximations in perspective.

In Chapter 3 we describe the code for calculating the zero range amplitude which must be subsequently modified for the finite range calculation.

In Chapter 4 we discuss the various possible methods for finite range calculation and derive the method most suitable for including the finite range corrections in the WBP model. We review the problems met in similar calculations including the calculation of non-local effects and finite range corrections to the DWBA.

In Chapter 5 the results of example calculations are presented for a variety of low-lying states on target nuclei ranging from oxygen to zirconium. The qualitative nature of the finite range corrections is discussed, including trends dependent on the atomic number and the

orbital angular momentum of the captured neutron. Changes in the spectroscopic factor, the most important effect, are listed. The nature of the finite range effects are shown to be similar to those of non-locality.

CHAPTER 2

THE BASIC ASSUMPTIONS OF THE WBP MODEL

In this chapter the physical assumptions which lead to the WBP model are discussed and a method for deriving the expression for the transition amplitude is outlined.†

An exact solution for a (d,p) reaction on a target nucleus of A nucleons depends upon 3A + 6 position coordinates plus spin and isospin coordinates. Stripping reactions which lead to low-lying states of the residual nucleus are thought to proceed mainly via a direct process in which the internal degrees of freedom of the target nucleus are left unexcited. Thus optical potentials are introduced to represent the effective interactions of the neutron and proton with the target nucleus and the many-body problem is reduced to a three-body problem.

While this reduction of the many-body problem leads to a simple concept of the reaction mechanism, it has the disadvantage that the parameters which characterize the optical potentials are not unique so that for each reaction a range of predictions can result. Since the three-body problem itself is difficult to solve, and since the parameter ambiguities for the optical potentials increase the need for computational simplicity, the WBP model introduces further approximations the

---

† The derivation outlined here does not make use of the wave function Θ^{+} which has non-physical boundary conditions[52]).

validity of which depends upon the weak binding of the deuteron and the small momentum transferred in the stripping reaction.

For simplicity, consider a (d,p) reaction in which the final state can be represented by a neutron in a single particle state bound to a spherical target nucleus core. For further simplicity, also neglect dependence on particle spins. Let H be the total Hamiltonian, E be the total energy, and $\Psi^{(+)}$ be the total wave function for the system. Let $A_j(\xi)$ be a complete set of eigenfunctions for the target nucleus corresponding to the Hamiltonian H_t, and $V_n(\vec{r}_n, \xi)$, $V_p(\vec{r}_p, \xi)$ represent the neutron-target nucleus and proton-nucleus interactions, respectively.

The initial state

$$\Phi_i = \varphi_d(\vec{r}_n - \vec{r}_p) \exp(i \vec{K}_d \cdot \vec{R}) A_0(\xi) \tag{1}$$

describes a free deuteron with momentum $\hbar \vec{K}_d$ incident on the target nucleus in its ground state A_0. The final state

$$\theta_f = \exp(i \vec{k}_p \cdot \vec{r}_p) B(\vec{r}_n, \xi) \tag{2}$$

describes a free proton with momentum $\hbar \vec{k}_p$ and a neutron bound to the target nucleus core. The transition amplitude from the initial to final state can be written in the form[85]

$$T_{fi} = \langle \Psi_f^{(-)} | V_{np} | \Psi^{(+)} \rangle \tag{3}$$

where $\Psi_f^{(-)}$ satisfies the equation

$$(H - V_{np} - E)\Psi_f^{(-)} = 0 \quad . \tag{4}$$

Because of the weak binding and extended nature of the deuteron, it is expected that the neutron will play a minor role in the scattering of the proton when they are both close to the target nucleus. With this in mind, we introduce a complete set of proton-target nucleus scattering states $\Phi_{j\vec{k}_p}(\vec{r}_p,\xi)$ and expand the wave functions $\Psi_f^{(-)}$, $\Psi^{(+)}$

$$\Psi_f^{(-)} = \sum_m \int d\vec{k}_{p'}\, v^-_{m\vec{k}_{p'}}(\vec{r}_n)\, \Phi^{(-)}_{m\vec{k}_{p'}}(\vec{r}_p,\xi) \tag{5}$$

$$\Psi^{(+)} = \sum_j \int d\vec{k}_{p''}\, \omega^+_{j\vec{k}_{p''}}(\vec{r}_n)\, \Phi^{(+)}_{j\vec{k}_{p''}}(\vec{r}_p,\xi) \tag{6}$$

where the superscripts (-) and (+) refer to incoming and outgoing boundary conditions, respectively.

The substitution of expressions (5) and (6) into the amplitude (3) leads to an exact expression for the transition amplitude. At this point we make the "optical" assumption[86]

$$\Phi^{(\pm)}_{j\vec{k}_p}(\vec{r}_p,\xi) \simeq \chi^{(\pm)}_{\vec{k}_p}(\vec{r}_p)\, A_j(\xi) \tag{7}$$

with

$$\int d\vec{k}_{p'}\, |\chi^{(\pm)}_{\vec{k}_{p'}}\rangle\langle\chi^{(\pm)}_{\vec{k}_{p'}}| \simeq 1 \tag{8}$$

which is necessary to reduce the many-body problem to a three-body problem. With the "optical" approximation (7) the exact expression for the transition amplitude reduces to

$$T_{fi} = \langle \chi^{(-)}_{\vec{k}_p}\, v^-_{o\vec{k}_p} | V_{np} | \int d\vec{k}_{p''}\, \chi^{(+)}_{\vec{k}_{p''}}\, \omega^+_{o\vec{k}_{p''}} \rangle \tag{9}$$

which becomes with the substitution (8)

$$T_{fi} = \int d\vec{k}_{p'}\, \mathbf{S}(\vec{k}_p,\vec{k}_{p'}) \langle v^-_{o\vec{k}_p}\, \chi^{(+)}_{\vec{k}_{p'}} | V_{np} | \int d\vec{k}_{p''}\, \chi^{(+)}_{\vec{k}_{p''}}\, \omega^+_{o\vec{k}_{p''}} \rangle \tag{10}$$

where $S(\vec{k}_p, \vec{k}_p') = \langle \chi^{(-)}_{k_p} | \chi^{(+)}_{k_p} \rangle$ is the usual S matrix for proton scattering as described by the optical model.

The equations satisfied by the coefficients $v_{o k_p}$ and $\omega_{o k_p}$ are obtained by substituting the expansions (5) and (6) respectively together with the "optical" assumptions (7) into the Schroedinger equations for $\Psi_f^{(-)}$ and $\Psi^{(+)}$. The coupled equations which result have the form

$$[T_n - (E - E_{o k_p})]\, v^-_{o k_p}(\vec{r}_n) + \sum_j \langle A_o(\xi) | V_n | A_j(\xi) \rangle\, v^-_{j k_p}(\vec{r}_n) = 0 \qquad (11)$$

and

$$[T_n - (E - E_{o k_p})]\, \omega^+_{o k_p}(\vec{r}_n) + \sum_j \langle A_o(\xi) | V_n | A_j(\xi) \rangle\, \omega^+_{j k_p}(\vec{r}_n) + \int d\vec{k}_{p''} \langle \chi^{(+)}_{k_p}(\vec{r}_p) | V_{np} | \chi^{(+)}_{k_{p''}}(\vec{r}_p) \rangle\, \omega^+_{o k_{p''}}(\vec{r}_n) = 0 \,. \qquad (12)$$

The equations (11) and (12) are identical in form except for the last term on the left of Eq. (12) which takes account of the interaction between the neutron and proton. The set of equations (11) for the various functions $v^-_{j k_p}$ can be projected onto the subspace of the $v^-_{o k_p}$ by means of the projectors[87] $P \equiv |A_o\rangle\langle A_o|$ and $Q \equiv 1 - P$. The single equation which results

$$[T_n - (E - E_{o k_p}) + \langle A_o | V_n | A_o \rangle]\, v^-_{o k_p} + \langle A_o | V_n Q [E - E_{o k_p} - Q(T_n + V_n) Q]^{-1} Q V_n | A_o \rangle\, v^-_{o k_p} = 0 \qquad (13)$$

refers to a neutron in an "effective interaction."

In keeping with our "optical" assumption, we replace this effective interaction by an optical potential. Since one can show that $E - E_{0k_p} = E_B$, the binding energy of the captured neutron, Eq. (13) reduces to

$$[T_n + V_{\text{optical}} - E_B]\, \upsilon^-_{0k_p} = 0 \tag{14}$$

where all the terms involved are independent of k_p.

Up to this point only "optical" assumptions have been made and the equations are essentially the exact "three-body" equations. The basic WBP model approximations center on the last term on the left of Eq. (12). The neutron capture factor in the transition amplitude (10), namely

$$K_{cap} = \langle \upsilon^-_{0k_p} \int d\vec{k}_p \cdot \chi^{(+)}_{k_p} \,|\, V_{np} \,|\, \chi^{(-)}_{k_{p''}} \omega^+_{0k_{p''}} \rangle = \langle \upsilon^-_{0k_p}(\vec{r}_n) \,|\, \Gamma(\vec{r}_n) \rangle \tag{15}$$

is the overlap of this term with the bound state wave function $\upsilon^-_{0k_p}$. In the system of equations (12) the second term on the left involves coupling between different excited states of the target nucleus. The last term involves coupling to states with different proton momentum $\hbar\vec{k}_{p''}$.

To understand the nature of this coupling, introduce the Fourier transform of the deuteron wave function

$$G(\vec{K}) = \frac{1}{(2\pi)^3} \int \Phi_d(\vec{p}) \exp(i\vec{K}\cdot\vec{p})\, d\vec{p} \quad . \tag{16}$$

In terms of this Fourier transform the initial state (1) can be written

$$\Phi_i = \int d\vec{K}\; G(\vec{K}) \exp(i\vec{k}_p \cdot \vec{r}_p) \exp(i\vec{k}_n \cdot \vec{r}_n)\, A_0(\xi) \tag{17}$$

where $\vec{k}_n + \vec{k}_p = \vec{K}_d$ and $\vec{K} = \frac{\vec{K}_d}{2} - \vec{k}_p$. Comparing the expressions (17) and (6) and using the optical assumption (7), we see that for $\vec{r}_p, \vec{r}_n \to \infty$

$$\chi^{(+)}_{\vec{k}_p}(\vec{r}_p) \longrightarrow (2\pi)^{-3/2} \exp(i\vec{k}_p \cdot \vec{r}_p)$$

and

$$\omega^{+}_{o\,\vec{k}_p}(\vec{r}_n) \longrightarrow (2\pi)^{-3/2} G(\vec{K}) \exp(i\vec{k}_n \cdot \vec{r}_n) \; . \qquad (18)$$

With the substitutions (18). the last term on the left of Eq. (12) becomes

$$\Gamma(\vec{r}_n) = \frac{1}{(2\pi)^{3/2}} \int d\vec{r}_p \exp(-i\vec{k}_p \cdot \vec{r}_p) V_{np}(\rho) \int d\vec{K}'' G(\vec{K}'') \exp(i\vec{k}_{p''} \cdot \vec{r}_p) \exp(i\vec{k}_{n''} \cdot \vec{r}_n) \qquad (19)$$

where $\vec{K}'' = \frac{\vec{K}_d}{2} - \vec{k}_{p''}$. Transforming to the coordinates $\vec{R}, \vec{\rho}$ this becomes

$$\Gamma(\vec{r}_n) = \frac{1}{(2\pi)^{3/2}} \int d\vec{r}_p \exp(-i\vec{k}_p \cdot \vec{r}_p) \exp(i\vec{K}_d \cdot \vec{R}) V_{np}(\rho) \int d\vec{K}'' G(\vec{K}'') \exp(i\vec{K}'' \cdot \vec{\rho}) \; . \qquad (20)$$

Since the last integral on the right of the expression (20) is the deuteron wave function $\phi_d(\rho)$ we can make use of the Schroedinger equation

$$\left[-\frac{\hbar^2}{m} \nabla_\rho^2 + \frac{\hbar^2 \gamma^2}{m} \right] \phi_d(\rho) = V_{np}(\rho)\, \phi_d(\rho) \qquad (21)$$

where $\frac{\hbar^2 \gamma^2}{m}$ is the deuteron binding energy and replace Eq. (20) with

$$\Gamma(\vec{r}_n) = \frac{1}{(2\pi)^{3/2}} \int d\vec{r}_p \exp(-i\vec{k}_p \cdot \vec{r}_p) \exp(i\vec{K}_d \cdot \vec{R}) (-\tfrac{\hbar^2}{m})(\nabla_\rho^2 + \gamma^2) \int d\vec{K}'' G(\vec{K}'') \exp(i\vec{K}'' \cdot \vec{\rho}) \; . \qquad (22)$$

Changing the order of differentiation and integration, this becomes

$$\Gamma(\vec{r}_n) = \frac{1}{(2\pi)^{3/2}} \int d\vec{K}'' d\vec{r}_p \exp(-i\vec{k}_p \cdot \vec{r}_p) \exp(i\vec{k}_{p''} \cdot \vec{r}_p) G(\vec{K}'') \left(-\frac{\hbar^2}{m}\right)(K''^2 + \gamma^2) \exp(i\vec{k}_{n''} \cdot \vec{r}_n)$$

$$= \frac{1}{(2\pi)^{3/2}} \int d\vec{K}'' \delta(\vec{k}_p - \vec{k}_{p''}) G(\vec{K}'') \left(-\frac{\hbar^2}{m}\right)(K''^2 + \gamma^2) \exp(i\vec{k}_n \cdot \vec{r}_n) \qquad (23)$$

$$= -\frac{\hbar^2}{m}(K^2 + \gamma^2)\, \omega^+_{o\vec{k}_p}(\vec{r}_n) \,. \qquad (24)$$

The result (24) shows that in the asymptotic incident beam the function $\omega^+_{o\vec{k}_p}$ in Eq. (12) is <u>not coupled</u> to states with different proton momentum $\hbar\vec{k}_{p''}$. The coupling term in Eq. (12) acts only in the vicinity of the target nucleus.

The basic WBP model approximation removed the coupling to states of different $\vec{k}_{p''}$ everywhere. The last term in Eq. (12) is replaced by a term which is equal to the right hand side of Eq. (24) in the asymptotic region and which is diagonal in k_p, i.e.,

$$\Gamma(\vec{r}_n) = \mathcal{V}^{\ell}(\vec{r}_n, \vec{k}_p)\, \omega^+_{o\vec{k}_p}(\vec{r}_n)$$

where

$$\mathcal{V}^{\ell}(\vec{r}_n, \vec{k}_p) = -(2\pi)^3 \frac{\hbar}{m}(K^2 + \gamma^2) \int d\vec{r}_p \, |\mathcal{V}^{(+)}_{\vec{k}_p}|^2(\vec{r}_p) V_{np}(\vec{r}_n - \vec{r}_p) \Big/ \int d\vec{r}_p \, V_{np}(\vec{r}_n - \vec{r}_p) \qquad (25)$$

Numerical calculations which justify the approximation (25) have been made[88]. The justification depends on the weak binding of the deuteron and on the small momentum transfers in the reaction.

To complete the discussion concerning the generation of the coefficients $\omega^+_{o\vec{k}_p}$ we rewrite the WBP approximation to Eq. (12) in

the form

$$\left[T_n - \left(E - E_{o k_p} + \frac{\hbar^2}{m}(K^2+\gamma^2)\right)\right]\omega^+_{o k_p}(\vec{r}_n) \qquad (26)$$
$$- \sum_j \langle A_o(\xi)\,|\,V_n\,|\,A_j(\xi)\rangle\,\omega^+_{j k_p}(\vec{r}_n) - \mathcal{V}^{\ell}_{SHORT}\,\omega^+_{o k_p}(\vec{r}_n) = 0$$

where

$$\mathcal{V}^{\ell}_{SHORT}(\vec{r}_n, \vec{k}_p) = \mathcal{V}^{\ell}(\vec{r}_n, \vec{k}_p) + \frac{\hbar^2}{m}(K^2+\gamma^2)$$

is a short-ranged potential being non-zero only in the vicinity of the target nucleus. Since

$$-E_{o k_p} + \frac{\hbar^2}{m}(K^2+\gamma^2) = \frac{\hbar^2 k_n^2}{2m} = E_{FREE}$$

is the energy of the free neutron, Eq. (26) becomes

$$\left[T_n - E_{FREE}\right]\omega^+_{o k_p}(\vec{r}_n) + \sum_j \langle A_o(\xi)\,|\,V_n\,|\,A_j(\xi)\rangle\,\omega^+_{j k_p}(\vec{r}_n) \qquad (27)$$
$$+ \mathcal{V}^{\ell}_{SHORT}(\vec{r}_n, \vec{k}_p)\,\omega^+_{o k_p}(\vec{r}_n) = 0 \quad .$$

Except for the last term on the left, the equations (27) have the same form as equations (11) for the $\psi^-_{o k_p}$. Since $\mathcal{V}^{\ell}_{SHORT}$ typically has a depth of $\simeq$ 2 MeV, we neglect it and as in equations (11) introduce an optical potential to take account of coupling to the excited states of the target nucleus. Thus, Eq. (27) becomes

$$\left[T_n - E_{FREE} - \mathcal{V}^{\ell}_{OPT}(\vec{k}_p, \vec{r}_n)\right]\omega^+_{o k_p}(\vec{r}_n) = 0 \quad . \qquad (28)$$

In the vicinity of the target nucleus $\mathcal{V}^{\ell}_{OPT} \simeq 60$ MeV so that the neglect of $\mathcal{V}^{\ell}_{SHORT}$ in Eq. (27) represents less than 5% of $\mathcal{V}^{\ell}_{OPT}$. Two WBP model calculations in which $\mathcal{V}^{\ell}_{OPT}$ is varied by 2 MeV give results which are essentially identical so that neglect of $\mathcal{V}^{\ell}_{SHORT}$ in Eq. (27) appears justified.

With the result (25) the expression (10) for the transition amplitude becomes

$$T_{fi} = \int d\vec{k}_p' \, S(\vec{k}_p, \vec{k}_p') \langle v^-_{0k_p}(\vec{r}_n) | \mathcal{V}(\vec{r}_n, \vec{k}_p) | \omega^+_{0k_p}(\vec{r}_n) \rangle \quad . \tag{29}$$

It is convenient to extract the asymptotic dependence of $\omega^+_{0k_p}(\vec{r}_n)$ on $\vec{k}_p$ by defining

$$u^+_{0k_p}(\vec{r}_n) = \omega^+_{0k_p}(\vec{r}_n)/G(\vec{K}) \tag{30}$$

so that

$$u^+_{0k_p}(\vec{r}_n) \longrightarrow (2\pi)^{3/2} \exp(i\vec{k}_n \cdot \vec{r}_n) \quad .$$

The function $u^+_{0k_p}(\vec{r}_n)$ is also a solution of Eq. (28). With the substitution (30), the expression (29) for the transition amplitude becomes

$$T_{fi} = \int d\vec{k}_p' \, G(\vec{K}) \, S(\vec{k}_p, \vec{k}_p') \langle v^-_{0k_p}(\vec{r}_n) | \mathcal{V}(\vec{r}_n, \vec{k}_p) | u^+_{0k_p}(\vec{r}_n) \rangle \quad . \tag{31}$$

This expression involves a nine-dimensional integration over the neutron coordinates $\vec{r}_n$, the proton coordinates $\vec{r}_p$ (in calculating $\mathcal{V}(\vec{r}_n, \vec{k}_p)$ through expression (25)), and the momenta $\vec{k}_p$. Because the interaction of the neutron on the proton is expected to be negligible compared to the interaction of the proton with the target nucleus, the WBP model includes only energy-conserving proton scattering in the amplitude (31). The amplitude (31) thus involves an eight-dimensional integration.

CHAPTER 3

WBP MODEL CALCULATIONS WITH THE ZERO RANGE APPROXIMATION

Since the method for dealing with the finite range problem which we describe in Chapter 4 leads to a relatively simple modification of the previous calculations made with the zero range approximation for V_{np}, we outline here some details of the method used for the zero range calculations and include a brief flow diagram for the computer program which performs the calculation. This helps in explaining how the finite range calculations are made. It also makes clear the advantage of a method for introducing finite range which does not alter the structure of the zero range calculations.

The eight-dimensional integral (29) is greatly simplified by means of the zero range approximation for V_{np}. With this approximation

$$V_{np}(\vec{r}_n - \vec{r}_p) = \int d\vec{p}\, V_{np}(\vec{p})\, \delta(\vec{r}_n - \vec{r}_p) \tag{32}$$

the interaction in Eq. (25) can be evaluated

$$\mathcal{V}(\vec{r}_n, \vec{k}_p) = -\frac{\hbar^2}{m}(K^2+\gamma^2)(2\pi)^3 \left|\chi^{(+)}_{\vec{k}_p}(\vec{r}_n)\right|^2 \tag{33}$$

and the integral in the amplitude (29) becomes five-dimensional.

$$T_{fi} = -\frac{\hbar^2}{m}(K^2+\gamma^2)(2\pi)^3 \int d\vec{k}_{p'}\, S(k_p, k_{p'})\, G(\vec{k}_{p'}, \vec{r}_d) \left\langle U_0(\vec{r}_n) \left| \chi^{(-)}_{\vec{k}_{p'}}(\vec{r}_n) \right| u_{0\vec{k}_p}(\vec{r}_n) \right\rangle . \tag{34}$$

The computation of Eq. (34) requires the calculation of the proton scattering matrix $S(\vec{k}_p, \vec{k}_{p'})$, the bound state neutron wave function

$v_o(\vec{r}_n)$, the incoming neutron wave function $u_{o\ell_p}(\vec{r}_n)$ and the density $|\chi^{(+)}_{\ell_p}|^2$ associated with the proton wave function. The calculation of each of these functions involves the solution of an equation such as (28) which is essentially a second order differential equation in three dimensions.

The solution of the differential equations and the integrations in Eq. (34) is simplified by using the method of partial waves. By expanding the wave functions in terms of spherical harmonics, the differential equations are reduced to one dimension. By expanding the proton density also in spherical harmonics, it becomes possible to analytically perform all but the radial integral over $\vec{r}_n$ and the integral over $\cos\theta_p$ in Eq. (34). The remaining integrals reduce to restricted sums of vector coupling coefficients. The details are given below.

Transition Amplitude for Particles with Spin

The previous discussion has not referred explicitly to the spin of the particles involved. For the simple case discussed in Chapter 2, we require the transition amplitude from the initial state in which the deuteron spin projection along the $\hat{z}$ axis is M_d to the final state for which the proton and neutron spin projections are μ_p and M_n, respectively.

The modifications necessary to take account of the particle spin can be seen as follows. They can be justified in a rigorous manner by going through a derivation similar to that in Chapter 2 in detail.

The expression (34) for the transition amplitude can be interpreted as follows: The incident deuteron is expressed through the

integral over $\vec{k}_{p'}$ as a packet of neutron-proton pairs, the proton with momentum $\hbar\vec{k}_{p'}$ and the neutron with momentum $\hbar\vec{k}_{n'}=\hbar(\vec{K}_d-\vec{k}_{p'})$. The proton is scattered via the S matrix from $\vec{k}_{p'}$ to $\vec{k}_p$ and the neutron is captured via the capture factor.

To take account of the particle spin we follow this interpretation and first express the deuteron spin function with total angular momentum projection μ_d in terms of neutron-proton pairs, the proton with spin projection $\mu_{p'}$ and the neutron with spin projection $\mu_{n'}$ such that $\mu_{n'}+\mu_{p'}=\mu_d$, the deuteron spin projection. The proton with spin projection $\mu_{p'}$ is then scattered via the matrix $S_{\mu_p\mu_{p'}}(\vec{k}_{p'},\vec{k}_p)$ to the state with spin projection μ_p and the neutron is captured with spin projection M_n.

The deuteron wave function in momentum space includes both an S-state and a D-state component

$$G^{m_d}(\vec{K}) = \tilde{u}(K)\left\{Y_0^0(\hat{K})\,|\,1\,m_d\rangle\right\} - \tilde{\omega}(K)\left\{\sum_{\mu_d}\langle 1\,m_d|1\mu_d\,2M\rangle\, Y_2^M(\hat{K})\,|\,1\mu_d\rangle\right\} \tag{35}$$

with

$$\tilde{u}(K) = 4\pi\int_0^\infty u(r)\, j_0(Kr)\, r\,dr$$

and

$$\tilde{\omega}(K) = 4\pi\int_0^\infty \omega(r)\, j_2(Kr)\, r\,dr \tag{36}$$

where $u(r)/r$ and $\omega(r)/r$ are the radial components of the deuteron S and D-state, respectively, and are normalized such that $\int_0^\infty (u^2+\omega^2)\,dr = 1$.

Defining

$$G_o^{\mu_d}(K) = \tilde{u}(K)\,|1\mu_d\rangle$$

and

$$G_2^{\mu_d}(K) = -\tilde{\omega}(K)\,|1\mu_d\rangle \tag{37}$$

in terms of these functions, the transition amplitude can be written as a sum of S-state and D-state terms.

$$T_{m_d \mu_p M_n} = {}^0T_{m_d \mu_p M_n} + {}^2T_{m_d \mu_p M_n}$$

where

$$\begin{aligned} {}^LT_{m_d \mu_p M_n} = \sum_{\mu_d \mu_{p'}} & \langle 1 m_d \,|\, L M \, 1 \mu_d \rangle \langle 1 \mu_d \,|\, \tfrac{1}{2} \mu_{p'} \, \tfrac{1}{2} \mu_{n'} \rangle \times \\ & \times \int d\vec{k}_{p'} \, G_L(\vec{K}_d, \vec{k}_{p'}) \, S_{\mu_{p'} \mu_p}(\vec{k}_{p'}, \vec{k}_p) \, Y_L^M(\Omega_K) \times \\ & \times \langle \psi^-_{M_n}(\vec{r}_n) \,|\, V^0(\vec{r}_n, \vec{k}_{p'}) \,|\, \psi^+_{\mu_{n'}}(\vec{r}_n, \vec{k}_{n'}) \rangle \; . \end{aligned} \tag{38}$$

As indicated in ref.[62]) it is possible to use a deuteron wave function derived from a "realistic" potential - one that fits two nucleon scattering data up to 300 MeV. The wave function presently used in WBP calculations is an analytic parameterization due to McGee[89]) of the wave function corresponding to the Hamada-Johnston[90]) potential.

The McGee parameterization for the momentum space wave function is

$$\tilde{u}_M(K) = 4\pi N_M \sum_{j=0}^{4} \frac{c_j}{K^2+\epsilon_j^2} \tag{39}$$

$$\tilde{w}_M(K) = 4\pi \rho N_M \sum \tag{40}$$

where the parameters ϵ_j, ϵ_j', c_j, c_j', γ, ρ, N_M are listed in Table 1.

Cross Section, Polarization and Analyzing Power

The differential cross section $d\sigma/d\Omega$ and polarization P_y calculated for an unpolarized beam can be expressed[52] in terms of the transition amplitudes (38) by

$$\frac{d\sigma}{d\Omega} = \frac{1}{3}\left(\frac{1}{2\pi\hbar^2}\right)^2 m_p^* m_d^* \frac{k_p}{k_d} \sum_{\mu_d \mu_p M_n} (T_{fi})^2_{\mu_d \mu_p M_n} \tag{41}$$

and

$$P_y = \frac{-2\,\mathrm{Im}\sum_{\mu_d M_n} (T_{fi})_{\mu_d \frac{1}{2} M_n} (T_{fi})^*_{\mu_d -\frac{1}{2} M_n}}{\sum_{\mu_d \mu_p M_n} |T_{fi}|^2_{\mu_d \mu_p M_n}} \tag{42}$$

The analyzing power P_D calculated for a vector polarized deuteron beam is given by[56]

$$P_D = \frac{\sqrt{2}\,\mathrm{Im}\sum_{\mu_p M_n}\left[(T_{fi})_{1\mu_p M_n}(T_{fi})^*_{0\mu_p M_n} - (T_{fi})_{0\mu_p M_n}(T_{fi})^*_{-1\mu_p M_n}\right]}{\sum_{\mu_p \mu_d M_n} |T_{fi}|^2_{\mu_d \mu_p M_n}} \tag{43}$$

The quantities m_p^* and m_d^* are the reduced masses of the proton and deuteron.

Table 1. Deuteron Wave Function Parameters from McGee

	S State		D State	
j	ε_j	C_j	ε'_j	C'_j
0	1.000γ	1.000	1.000γ	1.00
1	5.733γ	-0.63608	4.833γ	-20.34
2	12.844γ	-6.6150	10.447γ	-36.60
3	17.331γ	15.2162	14.506γ	-123.02
4	19.643γ	-8.9651	16.868γ	305.11
5			21.154γ	-126.16

$\gamma=0.2338\text{fm}^{-1}$, $N_M=0.8896\text{fm}^{-\frac{1}{2}}$, $\rho=0.0269$

The Partial Wave Expansions

The computation of the amplitudes (38) is simplified by using partial wave expansions. In the zero range expression for the neutron capture

$$\langle v_{M_n}(\vec{r}_n)\,|\,V(\vec{r}_n,\vec{k}_{p'})\,|\,u_{\mu_{n'}}(\vec{r}_n,\vec{k}_{n'})\rangle \tag{44}$$
$$= -(2\pi)^3\frac{\hbar^2}{m}\left(K'^2+\gamma^2\right)\int d\vec{r}_n\, v_{M_n}(\vec{r}_n)\,|\chi^+_{k_{p'}}(\vec{r}_n)|^2\, u_{\mu_{n'}}(\vec{r}_n,\vec{k}_{n'})$$

we write the final state

$$v_{M_n}(\vec{r}_n, j_n, l_n) = i^{l_n}\sum_{\mu_n}\langle \tfrac{1}{2}\mu_n\, l_n\, M_n-\mu_n\,|\,j_n\, M_n\rangle|\tfrac{1}{2}\mu_n\rangle Y_l^{M_n-\mu_n}(\Omega_n)\, v_{j_n l_n}(r_n) \tag{45}$$

where $|\frac{1}{2}\mu_n\rangle$ is the neutron spin function corresponding to the spin projection μ_n and $v_{j_n l_n}(r_n)$ represents the radial bound state wave function. The neutron scattering state $u_{\mu_{n'}}(\vec{r}_n,\vec{k}_{n'})$ which behaves as a plane wave in the asymptotic region may be written

$$u^+_{\mu_{n'}}(\vec{r}_n,\vec{k}_{n'}) = \frac{4\pi}{k_{n'}\, r_n}\sum_{j_{n'}\,l_{n'}\,M_{n'}\,\nu_n} i^{l_{n'}}\langle \tfrac{1}{2}\mu_{n'}\, l_{n'}\, M_{n'}\,|\,j_{n'}\, M_{n'}+\mu_{n'}\rangle \times \tag{46}$$
$$\times\langle \tfrac{1}{2}\nu_n\; l_{n'}\; M_{n'}+\mu_{n'}-\nu_n\,|\,j_{n'}, M_{n'}+\mu_{n'}\rangle\; Y^{*M_{n'}}_{l_{n'}}(\hat{k}_{n'})\times$$
$$\times\; Y^{M_{n'}+\mu_{n'}-\nu_n}_{l_{n'}}(\Omega_n)\;\chi^+_{j_{n'}\,l_{n'}}\,|\,\tfrac{1}{2}\nu_n\rangle\ .$$

The proton density in the interaction (33) may also be expanded in terms of spherical harmonics. Neglecting the small effects of the spin-orbit force on this density we express the proton wave function

$$\chi^+_{k_p}(\vec{k}_{p'},\vec{r}_n) = \sum_l \frac{i^l}{(2\pi)^{3/2}}(2l+1)\,\chi_l(k_{p'}, r_n)\,P_l(\cos\theta) \tag{47}$$

where we have chosen a coordinate system with z axis parallel to $\vec{k}_{p'}$.

The $\chi_\ell(r_n)$ corresponding to a particular angular momentum ℓ are the usual distorted wave functions describing elastic scattering of the proton from the target nucleus. Taking the modulus squared of Eq. (47) and making use of the identity[91])

$$P_\ell(\cos\theta)P_{\ell'}(\cos\theta) = \sum_{L,M} \frac{4\pi}{2L+1} \langle \ell 0 \ell' 0 | L 0 \rangle Y_L^{*M}(\hat{k}) Y_L^M(\hat{r}) \tag{48}$$

we obtain

$$(2\pi)^3 \left| \chi^+_{k_p}(\vec{r}_n) \right|^2 = \sum_{L,M} \frac{1}{2L+1} Y_L^{*M}(\hat{k}_{p'}) Y_L^M(\hat{r}_n) a_L(r_n) \tag{49}$$

where

$$a_L(r_n) = 4\pi \sum_{\ell\ell'} i^{(\ell-\ell')} (2\ell+1)(2\ell'+1) \langle \ell 0 \ell' 0 | L 0 \rangle^2 \chi_\ell(r_n) \chi^*_{\ell'}(r_n) \,. \tag{50}$$

With this expansion the capturing interaction (33) becomes

$$\mathcal{U}(\vec{r}_n, \vec{k}_{p'}) = -\frac{\hbar^2}{m}(K^2+\gamma^2) \sum_{L,M} \frac{a_L(r_n)}{2L+1} Y_L^M(\hat{r}_n) Y_L^{*M}(\hat{k}_{p'}) \,. \tag{51}$$

Although the expression (51) in principle contains an infinite sum over the orbital angular momentum L, in practice this summation is strongly restricted. From a study of the dependence of P_D, P_y and $d\sigma/d\Omega$ on the maximum value L_{max} it has been found that the summation can be truncated[61]) at $L_{max} = 6$. Larger values of L have little influence on the neutron capture partly because the coefficients a_L decrease in magnitude with increasing L, and partly because of the angular momentum coupling which is implied in the factor (44). The smallest allowed value for ℓ_n in the expansion (46) for the incoming neutron wave function is related to L and to the bound state angular

momentum l_n in the expression (45) by the triangle condition $l_{n'} \geq |L - l_n|$. Hence for $L = 7$ and $l_n = 1$ we have $l_{n'} \geq 6$. The partial waves with such a large value of $l_{n'}$ are small in the region where the bound state wave function is non-negligible.

Substitution of the expansions (45), (46), and (51) in the expression (44) for the neutron capture factor gives

$$\langle v^-(\vec{r}_n) | V(\vec{r}_n, \vec{k}_{p'}) | u_0^+(\vec{r}_n, \vec{k}_{n'}) \rangle = -\frac{\hbar^2}{m}(K^2+\gamma^2) K_{\mu_{n'} M_n}(\vec{k}_{p'}) \exp[-i(M_n - \mu_{n'})\phi_{p'}] \qquad (52)$$

where

$$K_{\mu_{n'} M_n}(\vec{k}_{p'}) = \pi^{-1/2} \sum_{\substack{\mu_n j_{n'} l_{n'} M_{n'} \\ L M}} \langle \tfrac{1}{2} \mu_n l_n M_n - \mu_n | j_n M_n \rangle \langle \tfrac{1}{2} \mu_{n'} l_{n'} M_{n'} | j_{n'} M_{n'} + \mu_{n'} \rangle \times \qquad (53)$$

$$\times \langle \tfrac{1}{2} \mu_n l_{n'} M_{n'} + \mu_{n'} - \mu_n | j_{n'} M_{n'} + \mu_{n'} \rangle (-)^{M_n - \mu_{n'}} i^{(l_{n'} - l_n)} (2 l_n + 1)^{1/2} (2L+1)^{-1/2} \times$$

$$\times (2 l_{n'} + 1)^{-1/2} \langle l_n 0 L 0 | l_{n'} 0 \rangle \langle l_n M_n - \mu_n L - M | l_{n'} M_{n'} + \mu_{n'} - \mu_n \rangle \times$$

$$\times k_{n'}^{-1} \int dr_n \, r_n \, a_L(r_n) \, v_{j_n l_n}(r_n) \, Y^+_{j_{n'} l_{n'}}(k_{n'} r_n) \times$$

$$\times \Theta_L^M(\cos\theta_{p'}) \, \Theta_{l_{n'}}^{M_{n'}}(\cos\theta_{n'})$$

and $\Theta_l^m(\cos\theta)$ is defined by

$$Y_l^m(\theta, \phi) = (2\pi)^{-1/2} \Theta_l^m(\cos\theta) \exp(im\phi)$$

$$\Theta_l^m(\cos\theta) = 0 \quad \text{if} \quad l < |m| \, .$$

As a result of the partial wave expansions (45), (46), and (51), the three-dimensional integral in the capture factor (44) has been reduced to the one-dimensional radial overlap integral

$$k_{n'}^{-1} \int dr_n \, r_n \, a_L(r_n) \, v_{j_n \ell_n}(r_n) \, \chi^{+}_{j_{n'} \ell_{n'}}(k_{n'} r_n)$$

and the summations involving the vector coupling coefficients in the expression (53).

To treat the scattering matrix S in a similar way, we first write it as a sum of two terms

$$S_{\mu_{p'} \mu_p}(\vec{k}_{p'}, \vec{k}_p) = \delta_{\mu_{p'} \mu_p} \delta(\vec{k}_{p'} - \vec{k}_p) - 2\pi i \, \delta(E_{p'} - E_p) \, T_{\mu_{p'} \mu_p}(\vec{k}_{p'}, \vec{k}_p) \, . \tag{54}$$

The second term on the right of the expression (54) can be expressed as a finite sum over partial waves. The term $\delta(\vec{k}_p - \vec{k}_{p'})$ cannot. We follow previous nomenclature[52]) in calling the first term on the right of Eq. (54) the "unscattered" amplitude and the remainder the "scattered" amplitude. Strictly speaking, the effects of proton scattering also appear in the "unscattered" amplitude through the neutron capturing amplitude (52).

Combining the first term of Eq. (54) with the expressions (38) and (52) we have for the unscattered term of the transition amplitude

$$T^{L\ \text{unscattered}}_{m_d \mu_p M_n} = \frac{\hbar^2 (K^2 + \gamma^2)}{\sqrt{2\pi}\, m} \sum_{\mu_d} \langle 1 \, m_d \, | \, L M \, 1 \mu_d \rangle \langle 1 \mu_d \, | \, \tfrac{1}{2} \mu_p \, \tfrac{1}{2} \mu_n \rangle \times \tag{55}$$

$$\times \, G^{\mu_d}(\vec{K}_d, \vec{k}_p) \, K_{\mu_n M_n}(\cos\theta_p) \, \Theta_L^{-M}(\cos\theta_p) \, .$$

To obtain the complete WBP amplitude we use the partial wave expansion for the proton scattering matrix

$$t_{\mu_{p'}\mu_p}(\vec{k}_{p'},\vec{k}_p) = \frac{-i\hbar^2}{2\pi m k_p}\sum_{jlm}\langle \tfrac{1}{2}\mu_{p'}\, l\, m \,|\, j\; m+\mu_{p'}\rangle \times \tag{56}$$

$$\times \langle \tfrac{1}{2}\mu_p\, l\, m+\mu_{p'}-\mu_p \,|\, j\; m+\mu_{p'}\rangle (\eta_{lj}-1)\times$$

$$\times Y_l^{*m}(\hat{k}_{p'})\, Y_l^{m+\mu_{p'}-\mu_p}(\hat{k}_p)$$

where the quantities η_{lj} are related to the complex phase shifts δ_{lj} for the total angular momentum $j = l \pm \frac{1}{2}$ by $\eta_{lj} = \exp(2i\delta_{lj})$. For the usual energies considered, $E_p \lesssim 20$ MeV and for $l \gtrsim 15$ the coefficients $(\eta_{lj}-1)$ tend to zero so that the summations over l, j, m are severely restricted. Combining the second term of Eq. (54) with the expressions (38), (52), and (56), the scattered term of the transition amplitude is

$$^{L}T^{\text{scattered}}_{m_d\mu_p M_n} = \frac{\hbar^2(K^2+\gamma^2)}{\sqrt{2\pi}\; m}\sum_{\substack{\mu_d\mu_{p'}\\ jlm}}\langle 1\, m_d \,|\, L\, M\, 1\mu_d\rangle\langle 1\mu_d \,|\, \tfrac{1}{2}\mu_{p'}\tfrac{1}{2}\mu_{n'}\rangle \times \tag{57}$$

$$\times\langle j\; m+\mu_{p'} \,|\, l\; m\; \tfrac{1}{2}\mu_{p'}\rangle\langle j\; m+\mu_{p'} \,|\, l\; m+\mu_{p'}-\mu_p\; \tfrac{1}{2}\mu_p\rangle\times$$

$$\times(\eta_{lj}-1)\int d(\cos\theta_{p'})\, K_{\mu_n M_n}(\cos\theta_{p'})\, \Theta_L^{-M}(\cos\theta_K)\, G_L^{\mu_d}(\cos\theta_{p'})\times$$

$$\times \Theta_l^{m}(\cos\theta_{p'})\, \Theta_l^{m+\mu_{p'}-\mu_p}(\cos\theta_p)\, \delta(m, M-M_n+\mu_{n'}) \,.$$

The complete WBP amplitude is then

$$(T_{fi})_{m_d\mu_p M_n} = \sum_{L=0,2}\left\{ {}^{L}T^{\text{unscattered}}_{m_d\mu_p M_n} + {}^{L}T^{\text{scattered}}_{m_d\mu_p M_n}\right\} . \tag{58}$$

Outline of Numerical Procedure

The global outline of the numerical procedure in calculating the amplitude may now be given. Shown in Fig. 2 is a schematic block diagram of the Fortran IV coding naming the key subroutines and the functions they compute.

1. Subroutine CGCS forms and stores the Clebsch-Gordan coefficients $\langle j_1 m_1 j_2 m_2 | JM \rangle$
2. Subroutine LGNDR computes the associated Legendre polynomials $\textcircled{H}_\ell^m(\cos\theta)$ needed in equations (53), (55), and (57).
3. Subroutine SCATFN reads the proton optical potentials and uses the Fox-Goodwin method[92,93]) to generate the proton wave functions $\chi_\ell^\pm(r_n)$ in the expression (50).
4. Subroutine BS generates the bound state wave function $u_{j_n \ell_n}(r_n)$ by an iterative procedure that guarantees the bound neutron have the correct binding energy.
5. Subroutine FASHFT calculates the phase shifts $\eta_{\ell j}$ of the proton scattering matrix (56) and the coefficients $a_L(r_n)$ of the proton density in expressions (49) and (50).
6. Subroutine OVRLAP reads the neutron optical potentials, generates the free neutron wave functions $\chi_{j_{n'} \ell_{n'}}(k_{n'} r_n)$ and computes the overlap integrals

$$I_{L j_{n'} \ell_{n'}}^{j_n \ell_n} = \frac{1}{k_{n'}} \int dr_n r_n a_L(r_n) u_{j_n \ell_n}(r_n) \chi_{j_{n'} \ell_{n'}}(k_{n'} r_n) \qquad (59)$$

for each angle $\theta_{p'}$.

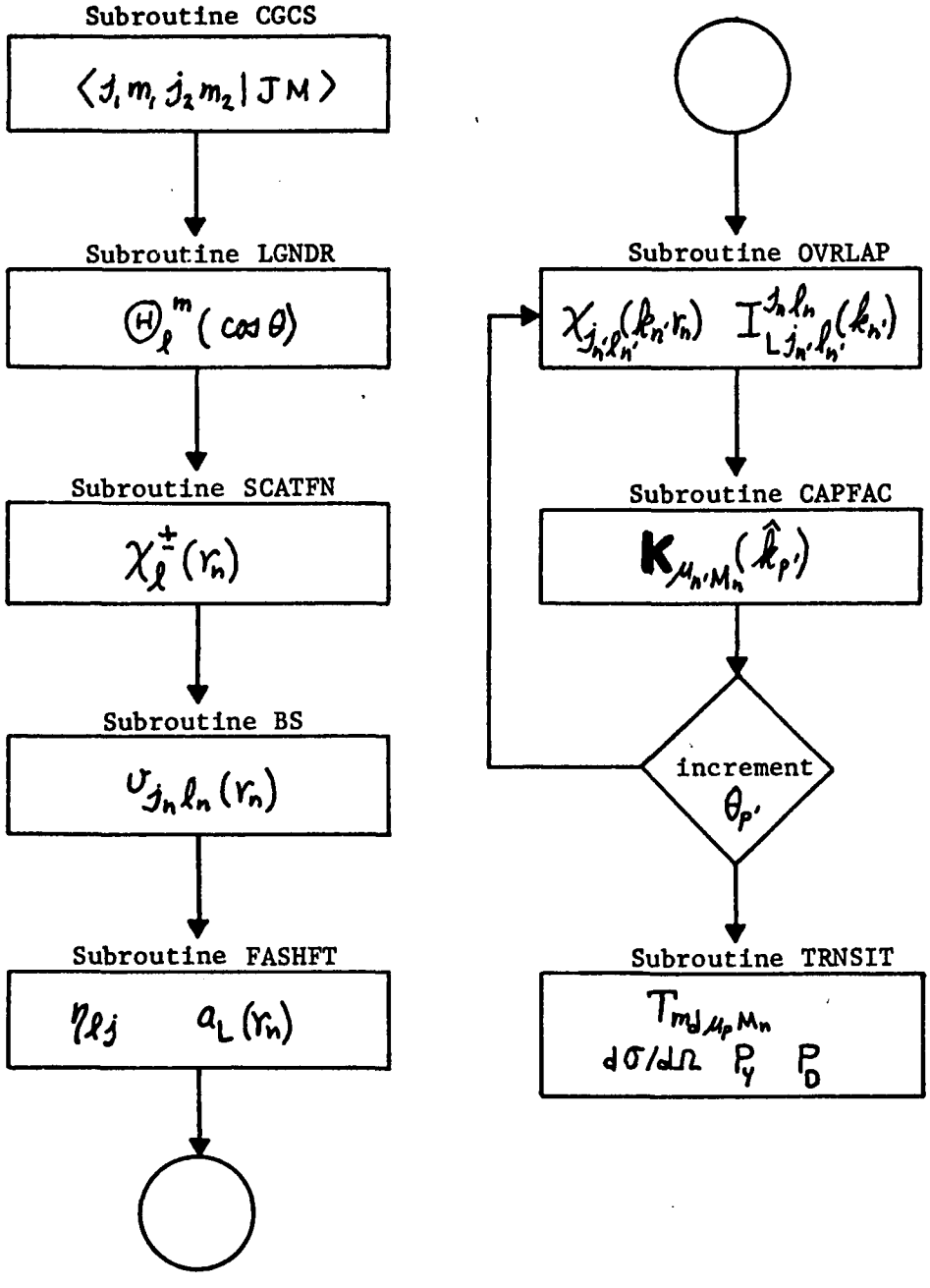

Fig. 2. Flow Chart for
Zero Range WBP Model Computations

7. Subroutine CAPFAC combines the vector coupling in Eq. (53) with the integral (59) to assemble the neutron capture factors $K_{\mu_n' M_n}(\cos\theta_{p'})$ for each angle $\theta_{p'}$.
8. Subroutine TRNSIT folds together the factors required to calculate the transition amplitudes given by the expressions (57) and (58). Since the amplitude (57) is a simple function of the outgoing angle θ_p, it is computed simultaneously for all values of θ_p.

A sizeable fraction of the time is spent executing subroutines OVRLAP and CAPFAC because they must be called for each value of $\theta_{p'}$. A typical computation time for an $l_n = 1$ case on an IBM 370/155 computer is 90 seconds CPU. The program size is 200,000 bytes of core.

CHAPTER 4

FINITE RANGE CORRECTIONS

Use of WBP model calculations to extract spectroscopic factors, to determine the total spin and to determine the parity of the final state in deuteron stripping reactions involves many calculations for different final states, target nuclei and bombarding energies. Since the optical model parameters with which the calculations are made are not determined unambiguously by elastic scattering, several calculations must be made for each case to understand the effects of the parameter ambiguities. Thus to provide a suitable tool for the analysis of stripping reactions the calculation of the WBP model amplitude must be reasonably economical. The zero range calculation described in Chapter 3 requires between one and two minutes on a medium-to-high speed fourth generation computer (IBM 370/155) and it is desirable that the finite range calculation should not substantially increase this time. This is especially so because finite range is expected to provide an important but small correction to the zero range amplitude. The success of the zero range calculations in fitting large bodies of angular distribution data suggests that the finite range corrections should not be of overwhelming importance except possibly in the extraction of accurate spectroscopic factors.

Need to Abandon the Integral ("Exact") Method

Because of the considerations given above the straightforward approach of integrating over the dimensions which were eliminated in the zero range treatment is not feasible. As indicated in Chapter 2 the WBP model amplitude

$$T_{fi} = \int d\Omega_{k_{p'}} \Lambda(k_{p'}) S(\vec{k}_{p'}, \vec{k}_p) \int d\vec{r}_n \, v(\vec{r}_n) w(\vec{r}_n) \int d\vec{s} \, V_{np}(\vec{s}) |\chi^+_{k_{p'}}|^2 (\vec{r}_n + \vec{s}) \qquad (60)$$

with

$$\Lambda = -(2\pi)^3 \frac{\hbar^2}{m} (K'^2 + \gamma^2) / \int d\vec{s} \, V_{np}(s)$$

involves an 8-dimensional integral. The integral over $\vec{s}$ in the expression (60) involves the proton density $|\chi^+_{k_{p'}}(\vec{r}_n + \vec{s})|^2$ throughout a volume of radius s_{max} (where s_{max} is the value of s for which $V_{np}(s)$ is non-zero) centered on the neutron coordinate $\vec{r}_n$. By making use of the spherical symmetry of $V_{np}(s)$ it is possible to reduce this integral to a single radial integral and some summations involving vector coupling coefficients. The zero range computation described in Chapter 3 already involves a two-dimensional numerical integration and vector coupling. Compared to the zero range calculation the straightforward finite range calculation would require a three-dimensional integration and more complicated vector coupling. We estimate that this would increase the time required for computation by at least an order of magnitude. A similar problem has been found with this approach to finite range calculations in the DWBA by Austern et al.[77]). In this case the increase in time required was approximately two orders of magnitude[80]).

Expansion Methods

As an alternative to the integral method referred to above one can try to separate the integrand in the amplitude (60) into a part which varies slowly with respect to one of the variables of integration and a part which varies rapidly. If this is possible one can expand the slowly varying part in a Taylor's series over the range of the rapidly varying part.

We consider two forms of the basic expansion method, one we call the configuration space method and the other the momentum space method.

Configuration Space Method

In the configuration space method one begins with the integral in expression (60) which has the symbolic form

$$I = \int d\vec{r}_n \int d\vec{s}\; D(s)\, J(\vec{r}_n + \vec{s}) \tag{61}$$

where $D(s)$ is an isotropic function of $\vec{s}$ which approaches zero rapidly for values of s greater than some range β. The function $J(\vec{r}_n + \vec{s})$ which varies slowly for values of $s < \beta$ is then expanded in a Taylor's series.

Using the translation operator $\exp(\vec{s}\cdot\vec{\nabla}_n)$ the function $J(\vec{r}_n + \vec{s})$ can be written in the form

$$J(\vec{r}_n + \vec{s}) = \exp(\vec{s}\cdot\vec{\nabla}_n)\, J(\vec{r}_n) \tag{62}$$

and the expression (61) as

$$I = \int d\vec{r}_n \left\{ \int d\vec{s}\; D(s) \exp(\vec{s}\cdot\vec{\nabla}_n)\, J(\vec{r}_n) \right\} . \tag{63}$$

The integration in braces can be performed as if the operator $\vec{\nabla}_n$ were an algebraic quantity. This formal integration is justified using Fourier transforms in Appendix A. When D is a function of scalar s only one obtains

$$\int s^2 ds \int d\Omega_s D(s) \exp(\vec{s}\cdot\vec{\nabla}_n) = 4\pi \int_0^\infty s^2 ds\, D(s) \frac{\sinh(s|\nabla_n|)}{s|\nabla_n|} \tag{64}$$

which with the series expansion

$$\sinh(x) = \sum_{m=0}^{\infty} \frac{x^{2m+1}}{(2m+1)!} \tag{65}$$

becomes

$$4\pi \int_0^\infty s^2 ds\, D(s) \frac{\sinh(s|\nabla_n|)}{s\nabla_n} = D_0 \sum_{m=0}^{\infty} \frac{\bar{s}^{2m}}{(2m+1)!} (\nabla_n)^{2m} \tag{66}$$

where

$$D_0 \equiv \int d\vec{s}\, D(s) \tag{67}$$

and

$$\bar{s}^{2m} \equiv D_0^{-1} \int d\vec{s}\, s^{2m} D(s) \tag{68}$$

are the 2m-th moments of the short ranged function $D(s,\beta)$.

In terms of the expressions (66), (67), and (68) the integral (63) becomes

$$I = D_0 \sum_{m=0}^{\infty} \frac{\bar{s}^{2m}}{(2m+1)!} \int d\vec{r}_n\, (\nabla_n)^{2m} J(\vec{r}_n)$$

$$= D_0 \left[\int d\vec{r}_n\, J(\vec{r}_n) + \frac{\bar{s}^2}{6} \int d\vec{r}_n\, (\nabla_n^2) J(\vec{r}_n) + \cdots \right] . \tag{69}$$

The convergence of the expansion (69) depends on the short range nature of the function $D(s)$ through its even moments and on the smoothness of the function $J(\vec{r}_n)$ through its even radial derivatives.

Momentum Space Method

In the momentum space method one expresses I in the form

$$I = \int d\vec{r}_n \int d\vec{K}\, \tilde{D}(K^2)\, \tilde{J}(\vec{r}_n, \vec{K}) \tag{70}$$

where

$$\tilde{D}(K^2) = \int d\vec{s}\, D(s) \exp(i\vec{K}\cdot\vec{s}) \tag{71}$$

and

$$\tilde{J}(\vec{r}_n, \vec{K}) = \int d\vec{s}\, J(\vec{r}_n + \vec{s}) \exp(i\vec{K}\cdot\vec{s}) \tag{72}$$

are the Fourier transforms of $D(s)$ and $J(\vec{r}_n+\vec{s})$, respectively. The function $\tilde{D}(K^2)$ depends only on the magnitude of K since $D(s)$ depends only on the magnitude of S.

In the momentum space method the roles of the functions D and J are reversed. When $D(s)$ is a peaked function of S over the range of which $J(\vec{r}_n+\vec{s})$ varies slowly, the Fourier transform $\tilde{J}(\vec{r}_n, \vec{K})$ is often a peaked function of $\vec{K}$ over the range for which $\tilde{D}(K^2)$ varies slowly. In this case $\tilde{D}(K^2)$ can be expanded[70] in a Taylor's series about some value α^2 which is chosen

to optimize the convergence of the expression (70). The result is

$$\tilde{D}(K^2) = \tilde{D}(\alpha^2) + (K^2 - \alpha^2)\tilde{D}'(\alpha^2) + \cdots \tag{73}$$

where

$$\tilde{D}'(\alpha^2) = \frac{\partial \tilde{D}(K^2)}{\partial K^2}\Big|_{K^2=\alpha^2} . \tag{74}$$

When $D(s)$ is expressed as the inverse Fourier transform of $\tilde{D}(K^2)$

$$D(s) = \left(\frac{1}{2\pi}\right)^3 \int d\vec{K}\, \tilde{D}(K^2) \exp(-i\vec{K}\cdot\vec{s}) \tag{75}$$

and the expansion (73) is substituted for $\tilde{D}(K^2)$ one finds

$$D(s) = \tilde{D}(\alpha^2)\delta(\vec{s}) - \tilde{D}'(\alpha^2)(\nabla_s^2 + \alpha^2)\delta(\vec{s}) + \cdots \tag{76}$$

where the property of the delta function

$$-\int K^2 d\vec{K}\, \exp(-i\vec{K}\cdot\vec{s}) = \nabla_s^2 \int d\vec{K}\, \exp(-i\vec{K}\cdot\vec{s}) \tag{77}$$

has been used. The expansion (76) can be used to evaluate the configuration space expression (61). One finds

$$\begin{aligned} I &= \int d\vec{r}_n \left\{ \tilde{D}(\alpha^2) J(\vec{r}_n) - (\nabla_s^2 + \alpha^2)\left[\tilde{D}'(\alpha^2) J(\vec{r}_n + \vec{s})\right]_{s=0} + \cdots \right\} \\ &= \int d\vec{r}_n \left\{ \tilde{D}(\alpha^2) J(\vec{r}_n) - \tilde{D}'(\alpha^2)\left[\nabla_n^2 + \alpha^2\right] J(\vec{r}_n) + \cdots \right\} . \end{aligned} \tag{78}$$

Correspondence Between Methods. The momentum and configuration methods are equivalent[70] when $D(s)$ is expanded about $S = 0$ and $\tilde{J}(\vec{r}_n, \vec{K})$ is expanded about $K = 0$. The first term of the expansion (78) can be evaluated by putting $K^2 = \alpha^2 = 0$ in the transform (71) to obtain

$$\tilde{D}(0) = \int d\vec{s}\, D(s) . \tag{79}$$

After some manipulation of the derivative of the transform (71) one obtains

$$\left.\frac{\partial \tilde{D}(K^2)}{\partial K^2}\right|_{K^2=0} = -\frac{1}{6}\int ds\, s^2 D(s) . \tag{80}$$

When the expressions (79) and (80) are inserted into the expansion (78) the result is

$$I = D_0\left[\int d\vec{r}_n\, J(\vec{r}_n) + \frac{\bar{s}^2}{6}\int d\vec{r}_n\, \nabla_n^2 J(\vec{r}_n) + \cdots\right] \tag{81}$$

which is identical to the expression (69).

The momentum space method gives a different expansion when $\tilde{D}(K^2)$ is expanded about some non-zero value K^2. However in this case it is essential that the value of $K^2 = \alpha^2$ which corresponds to the peak of $\tilde{J}(\vec{r}_n, \vec{K})$ can readily be determined. An example of expanding about a non-zero value of K^2 results from choosing α^2 so that the second term of the expression (78) vanishes. One obtains

$$0 = \tilde{D}'(\alpha^2)\left[\nabla_n^2 + \alpha^2\right] J(\vec{r}_n) . \tag{82}$$

In general the value of α^2 satisfying Eq. (82) will depend upon the coordinate $\vec{r}_n$. If one assumes the third and higher order terms of the expansion (78) are negligible[70,82] for this value of α^2, the integral I has the approximate value

$$I \simeq \int d\vec{r}_n \, J(\vec{r}_n) \, \tilde{D}(\alpha^2) \, . \tag{83}$$

Previous Experience With Expansion Methods

An integral of the form (61) occurs in the non-local form of the Schroedinger equation and in the DWBA stripping amplitude. The difficulties previously met in evaluating these integrals using expansion methods are briefly reviewed because they throw some light on the choice of the best method for evaluating the WBP model amplitude. A more detailed review is included in Appendix B. These difficulties previously met fall into two basic categories. We refer to them as the cross product difficulty and the evaluation of α^2 problem.

The cross product difficulty arises because the function J is usually a product of functions of the form

$$J(\vec{r}_n+\vec{s}) = F(\vec{r}_n+\vec{s}) \, G(\vec{r}_n+\tfrac{1}{2}\vec{s}) \, . \tag{84}$$

The translation operator $\exp(\vec{s}\cdot\vec{\nabla})$ then depends on the gradient operator

$$\vec{\nabla} = \tfrac{1}{2}\vec{\nabla}_1 + \vec{\nabla}_2$$

where $\vec{\nabla}_1$ acts only on G and $\vec{\nabla}_2$ only on F. In the power series expansion of the translation operator, terms with the form

$(\frac{1}{2}\vec{\nabla}_1 + \vec{\nabla}_2)^{2m}$ of higher order than first contain cross products $(\vec{\nabla}_1 \cdot \vec{\nabla}_2)^m$ which are extremely difficult to evaluate. This difficulty prevents the use of the configuration space method for solutions of the non-local Schroedinger equation, and for including finite range corrections to the DWBA transition amplitude beyond second order[82]. The second order corrections do not accurately estimate the finite range results[81].

The problem of evaluating α^2 occurs only with the momentum space method, for which α^2 should represent the value of K^2 at the peak of the function $J(\vec{r}_n, \vec{K})$. In the application of the method to solution of the non-local Schroedinger equation the value of α^2 is given the semi-classical value associated with a local potential. The cross product difficulty is avoided by ignoring derivatives of the function $G(\vec{r}_n + \frac{1}{2}\vec{s})$ which in this case corresponds to the symmetric non-local potential $U_N(\vec{r} + \frac{1}{2}\vec{s})$. Because of these two special circumstances the application of the momentum space method to non-local calculations has been quite successful[76].

In the application of the momentum space method to finite range DWBA calculations neither the cross product difficulty nor the evaluation of α^2 problem has been overcome. The function $J(\vec{r}_n + \vec{s})$ is the product of two wave functions

$$J(\vec{r}_n + \vec{s}) \longrightarrow \psi_p(\vec{r}_n + \vec{s})\, \psi_d(\vec{r}_n + \tfrac{1}{2}\vec{s}) \quad . \tag{85}$$

The derivative of neither Ψ_p nor Ψ_d can be neglected so the cross product difficulty is not avoided. In addition, accurate estimates of α^2 cannot be made[82]).

Application of Expansion Methods to Finite Range WBP Model Calculations

The WBP model transition amplitude (60) contains the integral

$$I = \int d\vec{r}_n \, v(\vec{r}_n) \, w(\vec{r}_n) \int d\vec{s} \, |\chi_p^+|^2 (\vec{r}_n + \vec{s}) \, V_{np}(s) \tag{86}$$

which has the same form as the integral (61) where

$$D(s) = V_{np}(s) \tag{87}$$

and

$$J(\vec{r}_n + \vec{s}) = |\chi_p^+|^2 (\vec{r}_n + \vec{s}) \; . \tag{88}$$

Application of the Momentum Space Method

Because $J(\vec{r}_n + \vec{s})$ in the expression (88) is the square of a wave function the calculation of expression (86) using the momentum space expansion method immediately encounters the difficulty of α^2. The problems are analogous to those previously encountered in evaluating the DWBA amplitude with this method[82]). It is not possible to avoid them as in the case of non-locality by using the semiclassical approximation which can be made only when J obeys the Schroedinger equation (see Appendix B). To see this we substitute the momentum space expansion (78) into expression (86) with the definitions (87) and (88) to

obtain

$$I = \int d\vec{r}_n \, v(\vec{r}_n) w(\vec{r}_n) \left\{ \tilde{V}_{np}(\alpha^2) |\chi_p^+|^2(\vec{r}_n) - \tilde{V}'_{np}(\alpha^2) [\nabla_n^2 + \alpha^2] |\chi_p^+|^2(\vec{r}_n) + \cdots \right] . \quad (89)$$

Setting the second term of the expansion (89) equal to zero and solving for $\alpha^2(\vec{r}_n)$ yields

$$\alpha^2(\vec{r}_n) = - \frac{\nabla_n^2 |\chi_p^+|^2(\vec{r}_n)}{|\chi_p^+|^2(\vec{r}_n)} \quad (90)$$

Thus α^2 is a complicated function of $\vec{r}_n$ which cannot be readily expanded in spherical harmonics as required if the expression (89) is to reduce to a one-dimensional integral.

The use of Green's theorem to transform the integral (89) does not result in a simple choice of α^2 . Using the result

$$\int d\vec{r}_n \, v(\vec{r}_n) w(\vec{r}_n) \tilde{V}'_{np}(\alpha^2) \nabla_n^2 |\chi_p^+|^2(\vec{r}_n) = \int d\vec{r}_n |\chi_p^+|^2(\vec{r}_n) \nabla_n^2 [v(\vec{r}_n) u(\vec{r}_n) \tilde{V}'_{np}(\alpha^2)] \quad (91)$$

one obtains the prescription

$$\alpha^2(\vec{r}_n) = - \frac{\nabla_n^2 [v(\vec{r}_n) w(\vec{r}_n)]}{v(\vec{r}_n) w(\vec{r}_n)} . \quad (92)$$

Not only is α^2 a complicated function of $\vec{r}_n$, but one encounters the cross product difficulty in evaluating it.

Application of the Configuration Space Method

The configuration space expansion of the integral (86) avoids both the difficulty associated with cross products and the evaluation of α^2 . Substituting the expansion (69) with the definitions (87) and (88) yields

$$I = V_0 \int d\vec{r}_n \, v(\vec{r}_n)\, w(\vec{r}_n) \sum_{m=0}^{\infty} \frac{\bar{s}^{2m}}{(2m+1)!} \left(\nabla_n^2\right)^m \left|\chi_p^+\right|^2(\vec{r}_n) \tag{93}$$

where

$$V_0 = \int d\vec{s}\, V_{np}(s)$$

and

$$\bar{s}^{2m} = V_0^{-1} \int d\vec{s}\, s^{2m} V_{np}(s) \quad .$$

To evaluate the derivatives in expression (93) we write the Laplacian in spherical polar coordinates

$$\nabla^2 = \left[\frac{1}{r} \frac{\partial^2}{\partial r^2} r + \frac{\hat{L}^2}{\hbar^2 r^2} \right] \tag{94}$$

where

$$\hat{L}^2 = -\frac{\hbar^2}{\sin^2\theta} \left[\sin\theta \frac{\partial}{\partial\theta} \left(\sin\theta \frac{\partial}{\partial\theta} \right) + \frac{\partial^2}{\partial\phi^2} \right] \tag{95}$$

and introduce the expansion (49) of $\left|\chi_p^+\right|^2(\vec{r}_n)$ in terms of spherical harmonics. The integral (93) becomes

$$I = (2\pi)^3 V_0 \int d\vec{r}_n \, v(\vec{r}_n) w(\vec{r}_n) \sum_{L,M} \frac{b_L(r_n)}{2L+1} Y_L^{*M}(\hat{k}_p)\, Y_L^M(\hat{r}_n) \tag{96}$$

where the coefficients $b_L(r_n)$ are given in terms of the zero range coefficients $a_L(r_n)$ of expression (50) by

$$b_L(r_n) = \frac{1}{r_n} \sum_{m=0}^{\infty} \frac{\bar{s}^{2m}}{(2m+1)!} \left[\frac{\partial^2}{\partial r_n^2} - \frac{L(L+1)}{r_n^2} \right]^m \left[r_n a_L(r_n) \right] \tag{97}$$

and contain only radial derivatives. The term with $m = 0$ in this expansion is the coefficient $a_L(r_n)$ which when substituted into the integral (96) gives the zero range approximation for the integral

$$I = \frac{V_0}{(2\pi)^3}\int d\vec{r}_n\, U(\vec{r}_n)\omega(\vec{r}_n)\sum_{LM}\frac{a_L(r_n)}{(2L+1)}\, Y_L^{*M}(\hat{k}_p)\, Y_L^M(\hat{r}_n) \quad . \tag{98}$$

The coefficients $b_L(r_n)$ in expression (97) are regular at the origin. The zero range functions $a_L(r_n)$ from which they are derived are defined by expression (50) in terms of the wave functions $\chi_\ell(r_n)$ which are the solutions of the radial Schroedinger equation in a central potential. For small values of $\rho = k_n r_n$ the power series expansion for the χ_ℓ has the form (see Appendix C)

$$\chi_\ell(r_n) \propto r_n^\ell \sum_{m=0}^{\infty} B_m r_n^{2m}, \qquad k_n r_n << 1 \tag{99}$$

where the summation contains only even powers of r_n . The vector coupling coefficient in expression (50) requires that $(\ell+\ell'-L)$ be even and non-negative, so that the power series expansion for the coefficients $a_L(r_n)$ has the form

$$a_L(r_n) \propto r_n^\ell \sum_{m=0}^{\infty} A_m r_n^{2m}, \qquad k_n r_n << 1 \quad . \tag{100}$$

Inserting the series (99) into the expression (97) gives after some manipulation (see Appendix C)

$$\frac{1}{r_n}\left[\frac{\partial^2}{\partial r_n^2} - \frac{L(L+1)}{r_n^2}\right]^k (r_n a_L(r_n)) \propto \sum_{m=k}^{\infty} A_m 2^k (m-k+1)(m-k+2)\times\cdots\times(m)\times$$
$$\times(2m+2L+1-2k+2)(2m+2L+1-2k+4)\times$$
$$\times\cdots\times(2m+2L+1)\, r_n^{2m+L-2k} \quad . \tag{101}$$

The lowest power of r_n in the series (100) is associated with $m = \ell$ and is proportional to r_n^L so that $b_L(r_n)$ is regular at the origin.

The coefficients (97) are expressed in terms of the even moments

$$\bar{s}^{2m} = 4\pi V_o^{-1} \int ds\, V_{np}(s)\, s^{2m+2} \qquad (102)$$

of the potential V_{np}. For the common short range central potential forms such as Yukawa, Gaussian and square well, these even moments (102) are finite for all values of m (see Table 2) and can be obtained in analytic form.

To compute the coefficients $b_L(r_n)$ the differentiation in the expression (97) is carried out numerically. This is simple to incorporate into the zero range WBP code since the coefficients $r_n a_L(r_n)$ are already stored for evaluating the overlap integrals (59) in the factor (55). Since the integral (96) has the same form as the zero range result (98) where the coefficients $a_L(r_n)$ have been replaced by the $b_L(r_n)$, one simply constructs the b_L and inserts them in place of the a_L.

The modifications are made by entering the subroutine FASHFT where the proton density coefficients $a_L(r_n)$ are constructed as indicated in the global outline in Fig. 2. This subroutine is passed through only once for each reaction - it is not reentered for each angle for the outgoing particle or each of the integration angles in the expression (60).

The coefficients $a_L(r_n)$ are typically computed for seven values of L and 100 values of r_n spaced in steps of 0.2 fm. When

Table 2. Comparison of Even Moments for Some Explicit Forms of V_{np} with Parameters Adjusted to Give a Triplet Effective Range $r_{e,t} = 1.7\text{fm}$ and a Triplet Scattering Length $a_t = 5.4\text{fm}$

Potential	Yukawa	Gaussian	Square Well
Form	$V_{np} = V_y \exp(-\gamma r)/\gamma r$	$V_{np} = V_g \exp(-\eta^2 r^2)$	$V_{np} = V_s$, $r \leq \nu^{-1}$ $V_{np} = 0$, $r > \nu^{-1}$
Range Parameter	$\gamma^{-1} = 1.5\text{fm}$	$\eta^{-1} = 1.5\text{fm}$	$\nu^{-1} = 2\text{fm}$
$\bar{s}^{2m}/(2m+1)!$	γ^{-2m}	$(m!)^{-1}(2\eta)^{-2m}$	$3(2m+3)^{-1}\{(2m+1)!\}^{-1}\nu^{-2m}$
$\dfrac{\bar{s}^{2m+2}/(2m+3)!}{\bar{s}^{2m}/(2m+1)!}$	$\gamma^{-2} \simeq 2.4\text{fm}^2$	$\{4\eta^2(m+1)\}^{-1}$ $\simeq 0.55\text{fm}^2/(m+1)$	$\nu^{-2}/(4m^2+14m+10)$ $\simeq 2.0\text{fm}^2/(2m^2+7m+5)$

the summation in (97) is truncated at the eighth derivative the numerical differentiation involved in (97) must be carried out 100x7x4 = 2800 times. This involves an insignificant increase in the computing time, typically less than 5%.

CHAPTER 5

NUMERICAL EXAMPLES

To carry out the finite range calculations some form must be chosen for the central potential $V_{np}(s)$. Since the neutron-proton relative momentum $\hbar K$ involved in the amplitude (60) corresponds to an energy which is typically $\leq$ 10 Mev[62]) the potential V_{np} should be chosen to fit the low energy nucleon-nucleon scattering data. It is known that one can fit low energy scattering data by a variety of potentials specified by two parameters[94]) which are adjusted to reproduce the experimental values of the triplet effective range $r_{e,t}$ and the scattering length a_t[95]). Thus the choice of potential is ambiguous. In order that the finite range predictions do not reflect this ambiguity it is necessary to use several forms of V_{np} and show that they give the same result in the WBP model calculations.

The number of terms which can be included in the expansion (97) for b_L is limited by the accuracy with which the successive numerical differentiations can be performed. In practice up to the eighth derivative can be retained. For a detailed discussion of the numerical methods used and the tests employed to check the accuracy see Appendix D. It is necessary to show that the WBP model amplitude evaluated with the expansion (97) has converged with this limited number of terms for each potential used.

The magnitude of the finite range corrections and the convergence of the expansion (97) is determined by the even moments $\bar{s}^{2m}$ which depend on the form and the range parameter for each potential V_{np}. If the WBP model amplitude can be shown to converge to a result which is independent of the shape of the potential used, then it will be convenient to choose the form of V_{np} for which the convergence is most rapid.

Several simple potential forms with two parameters adjusted to fit the triplet scattering length a_t and the effective range $r_{e,t}$ have been used to test the dependence of the finite range corrections on the potential shape and to check the convergence. In Table 2 the range parameters which are consistent with experimental values[95]) for a_t and $r_{e,t}$ are shown for the Yukawa, Gaussian and square well potentials. The values of the $2m$-th moments for these potentials are also listed together with the ratio $[\bar{s}^{2m+2}/(2m+3)!]/[\bar{s}^{2m}/(2m+1)!]$ of successive coefficients in the expansion (97).

In comparing the relative rates of convergence of (97) for the three forms it can be seen from Table 2 that the ratio of successive coefficients $[\bar{s}^{2m+2}/(2m+3)!]/[\bar{s}^{2m}/(2m+1)!]$ is smallest for the square well, Gaussian and Yukawa in that order for all values of m. The expansion (97) therefore converges most rapidly (if it does converge) for the three potentials in the same order. Thus if shape independence of finite range corrections can be demonstrated the square well would be the most convenient form to use.

Testing for Convergence and Shape Independence

Typical corrections to the coefficients $b_L(r_n)$ from the successive terms in the expansion (97) are shown in Fig. 3 as functions of r_n for the case corresponding to a square well potential with range ν^{-1} =2.0 fm. The corrections are smallest for $r_n > 5$ fm. This is the region which contributes most to the stripping amplitude. For almost all values of r_n the contributions to each b_L can be seen to decrease rapidly with increasing m .

The coefficients $b_L(r_n)$ are folded into the amplitude (60) from which the values for P_D, P_y and $d\sigma/d\Omega$ are obtained. Calculating the corrections to the values for P_D, P_y and $d\sigma/d\Omega$ from the various terms with different values of m in the expansion (97) involves a summation over L in the expression (96) and an integration over r_n in the amplitude (60). In this procedure the contributions from those regions of r_n space where the expansion (97) does not converge rapidly are averaged with contributions from those regions where the convergence is rapid.

The corrections to the values for P_D, P_y and $d\sigma/d\Omega$ corresponding to the second, fourth, sixth and eighth moments $\bar{S}^{2m}$ in the expansion (97) have been calculated for a variety of stripping reactions. Using a square well potential with range ν^{-1} = 2.0 fm it was found that corrections corresponding to $\bar{S}^2$, $\bar{S}^4$, $\bar{S}^6$ and $\bar{S}^8$ decreased successively by an order of magnitude for each increase of 2 in the order of the moments. Figure 4 shows typical effects on P_D and $d\sigma/d\Omega$ of truncating the expansion (97) for successively higher values of m . The curves for cross section and analyzing power coincide with solid

Fig. 3. Typical Finite Range Corrections
to the Coefficients $b_L(r)$ as a Function of r

The case corresponds to the reaction $^{40}Ca(d,p)^{41}Ca$ (1.95MeV p3/2) at E_d = 11MeV calculated with the parameters indicated in Table 5 for a square well potential V_{np} of range ν^{-1} = 2fm. The upper curves on the left show the terms with m = 1 and m = 2 in the expansion (97) for b_o as fractions of the zero range coefficient a_o. The remaining curves result from truncating the expansion (97) for each L at m = 0 (broken dotted curve corresponding to the zero range approximation), at m = 1 (solid curve) and at m = 2 (broken curve). All curves coincide with solid curves except where shown.

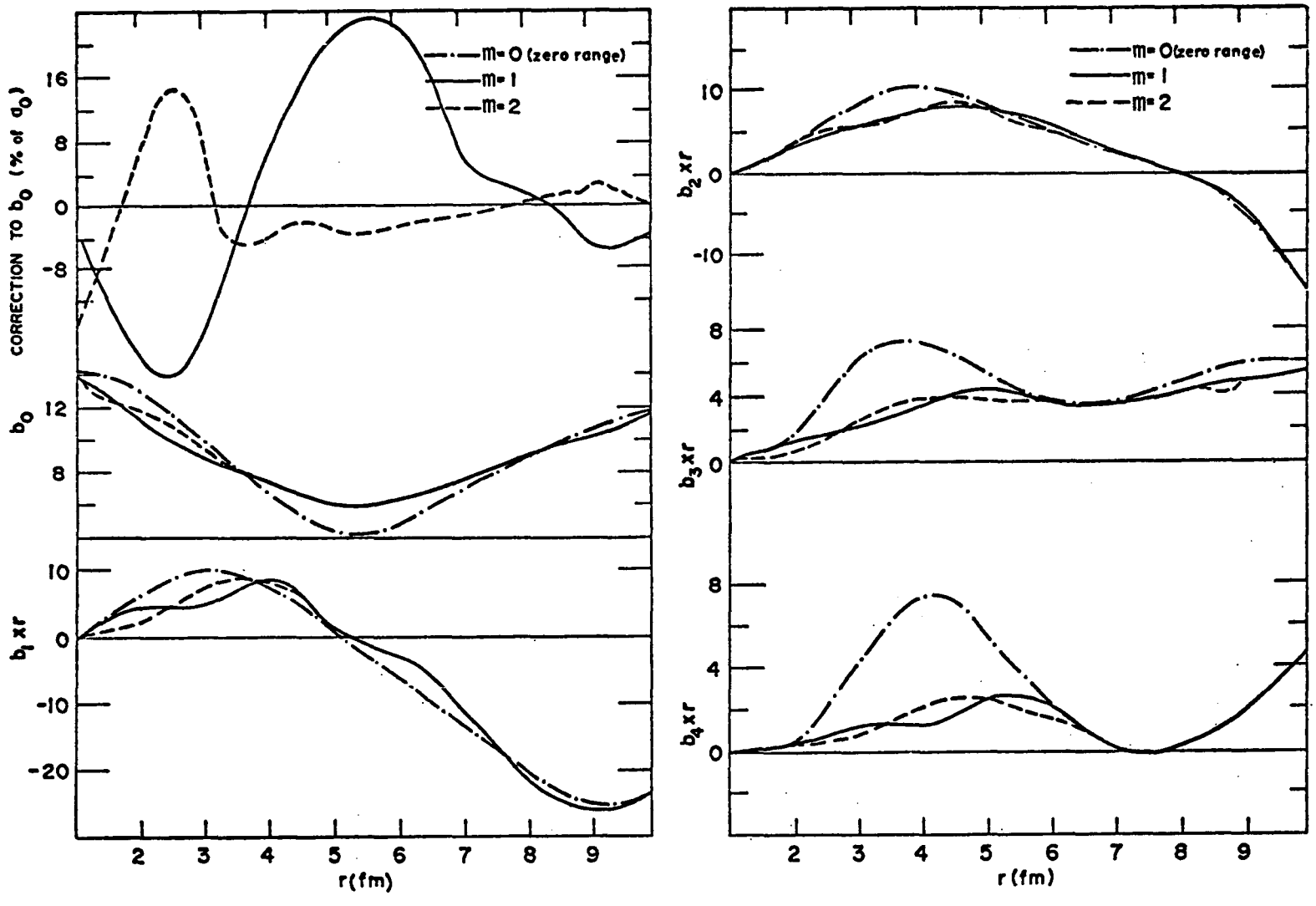

Fig. 3. Typical Finite Range Corrections to the Coefficients $b_L(r)$ as a Function of r

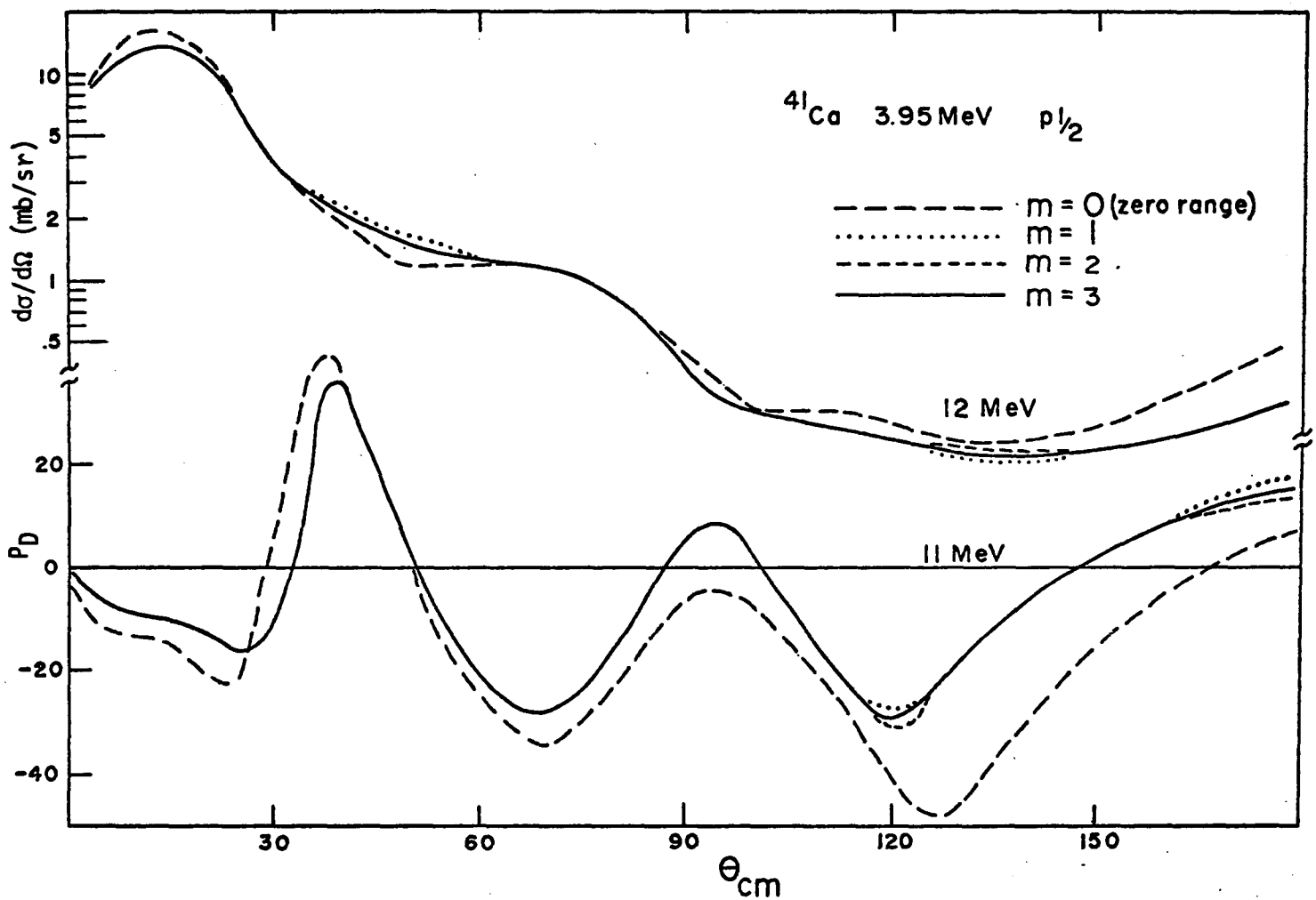

Fig. 4. Convergence of the Finite Range Expansion

curves where not shown. The correction to the zero range result from the term with $m = 1$ is significant. However the contributions from terms with higher values of m decrease rapidly with increasing m. It has been observed that corrections to P_D, P_y and $d\sigma/d\Omega$ due to successive powers of m alternate in sign. For example the corrections to the cross section in Fig. 4 near 135 degrees for $m = 1$, 2 and 3 are negative, positive and negative, respectively. Truncating the expansion (97) at $m = 1$ overemphasizes the finite range correction.

For the Gaussian potential with range $\eta^{-1} = 1.5$ fm the sequence of corrections to (97) corresponding to $\bar{s}^2$, $\bar{s}^4$ and $\bar{s}^6$ (see Table 3) decreased less rapidly than for the square well. While the calculated values for P_D, P_y and $d\sigma/d\Omega$ for the square well potential appear to have converged for $m = 3$, calculations with the Gaussian potential require the addition of the term with $m = 4$.

Table 3. Comparison of the Second Through Eighth Moments $\bar{s}^{2m}/(2m+1)!$ as Given in Table 2

m	moment	Yukawa	Gaussian	square well
1	2nd (fm^2)	2.4	0.56	0.4
2	4th (fm^4)	5.6	0.156	0.057
3	6th (fm^6)	13.3	0.029	0.004
4	8th (fm^8)	31.4	0.004	0.0002

With these truncations the values for P_D, P_y and $d\sigma/d\Omega$ calculated with the Gaussian and square well potentials are virtually identical. A comparison for a typical case is shown in Fig. 5. Since the finite range corrections do not depend on the shape of V_{np} we have chosen to use for the remainder of our calculations the square well potential which gives the most rapid convergence.

The square well and Gaussian potentials have short tails so that with parameters chosen to fit low energy two-nucleon scattering the weighted moments as shown in Table 3 form a rapidly decreasing sequence. For potentials such as the Yukawa potential which has an extended tail, the weighted moments may form an increasing sequence as shown in Table 3, and the expansion (97) may not converge. For such potentials our expansion method is not feasible.

Choice of Parameters

To study the nature of the finite range corrections it is necessary to choose carefully the parameters which specify the optical potentials which represent the interactions in Fig. 1. The details of the finite range corrections depend somewhat on these parameters. The optical potential parameters are found by fitting nucleon-nucleus scattering and bound state data. We use the values found for previous calculations with the zero range form of the WBP model.

To determine the bound state radial wave function $u_{j_n l_n}(r_n)$ we have used the potential

$$V_B(r) = V_0 \left[F(r) - \alpha \left(\frac{\hbar}{2mc}\right)^2 \frac{1}{r} \frac{dF}{dr} \vec{\sigma} \cdot \vec{l}\right] \tag{103}$$

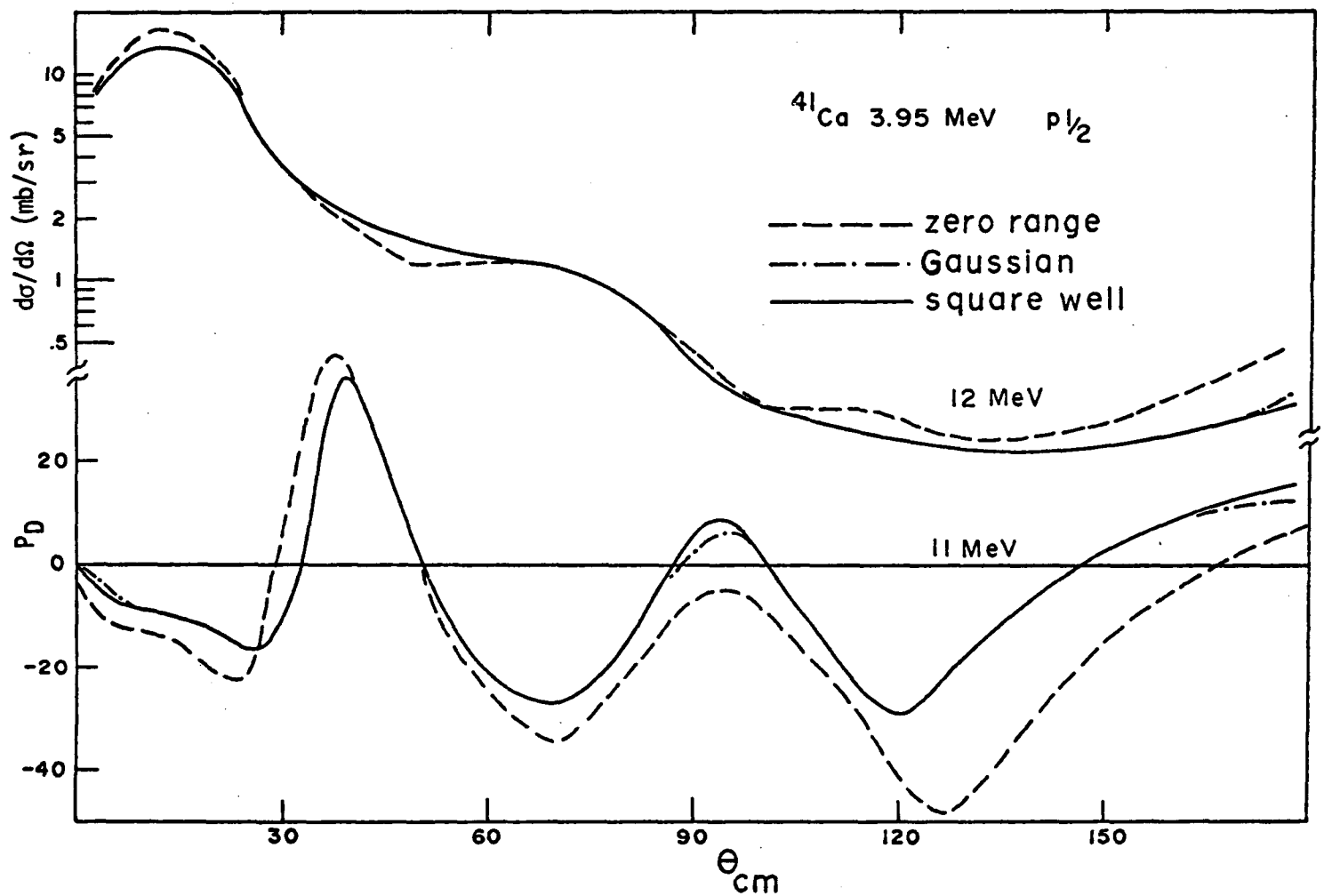

Fig. 5. Shape Independence of the Finite Range Correction

where $F(r)$ has the Woods-Saxon form

$$F(r) = \left[1 + \exp(r-R)/a\right]^{-1} . \tag{104}$$

In all cases we have used $\alpha = 32$, $R = 1.25A^{1/3}$ and $a = 0.65$ fm. The depth parameter V_0 is varied to reproduce the experimental binding energy.

The optical potentials for the scattered wave functions have the form

$$V(r) = -V F(r, a, r_a) - iW g(r) - i W_V F(r, b, r_b) - V_s h(r)\vec{\sigma}\cdot\vec{l} + V_c(r) \tag{105}$$

with

$$F(r, a, r_a) = \left[1 + \exp\left(\frac{r-R}{a}\right)\right]^{-1}, \quad R = r_a A^{1/3} \tag{106}$$

and

$$g(r) = -4b \frac{d}{dr} F(r, b, r_b) , \quad R = r_b A^{1/3} \tag{107}$$

and

$$h(r) = -\lambda_\pi^2 r^{-1} \frac{d}{dr} F(r, c, r_c) , \quad \lambda_\pi \approx \sqrt{2}\ \text{fm}, \quad R = r_c A^{1/3} . \tag{108}$$

The proton potential was truncated as in ref.[52]). The Hamada-Johnston form of the deuteron wave function is used as in ref.[62]). Non-local corrections to the neutron and proton wave functions are made by dividing each wave function by the factor (see Eq. (B15) in Appendix B)

$$f(r) = \left[1 - \frac{m\beta^2}{2\hbar^2} U_L(r)\right]^{1/2} \tag{109}$$

where β is the non-locality parameter and $U_L(r)$ is the appropriate neutron or proton local optical potential. Note that $f \to 1$ for large r while $|f| < 1$ in the nuclear interior. This damping of the nuclear interior increases with increasing β. For the standard case we choose $\beta = 0.85$.

The calculations reported here are based on the average optical-model parameters of either Rosen et al.[96]) or Becchetti and Greenlees[97]) (referred to as "BG") with small modifications for each target nucleus. The Rosen and BG parameters are listed in Table 4 and the parameter sets used for each reaction are listed in Table 5.

Qualitative Nature of the Finite Range Corrections

Typical finite range corrections to the values calculated for P_D, P_y and $d\sigma/d\Omega$ are shown in Figs. 6-12 for reactions with $\ell_n = 0$, 1, 2 and 3 on target nuclei ^{16}O, ^{40}Ca and ^{90}Zr. The data shown for these reactions were taken from refs.[98-105]) as indicated in Table 6. These reactions were previously used to test WBP model calculations with the zero range approximation[56,61]) which reproduced the main features of the measurements for P_D, P_y and $d\sigma/d\Omega$ over a range of deuteron energy. It is of some interest to see whether the finite range corrections improve the fits to the data especially in any systematic way. It is also interesting to compare the finite range effects in the WBP model with corresponding effects in DWBA calculations and in non-locality.

In the two previous cases where an integral of the form (60) was evaluated by expansion methods, namely for the evaluation of wave functions in a non-local potential and for calculating the DWBA

Table 4. Optical Model Parameters of Rosen and Becchetti-Greenlees

	Rosen		Becchetti-Greenlees (BG)	
	Neutron	Proton	Neutron	Proton
V (MeV)	49.3-0.33E	53.8-0.33E	56.3-0.32E	$54.0-0.32E + 0.4ZA^{-1/3}$
W (MeV)	5.75	7.5	13.0-0.25E or zero	11.8-0.25E or zero
W_V(MeV)	0.	0.	0.22E-1.56 or zero	0.22E-2.7 or zero
a(fm)	0.65	0.65	0.75	0.75
b(fm)	0.70	0.70	0.58	0.51
c(fm)	0.65	0.65	0.75	0.75
r_a(fm)	1.25	1.25	1.17	1.17
r_b(fm)	1.25	1.25	1.26	1.32
r_c(fm)	1.25	1.25	1.01	1.01
V_S(MeV)	5.5	5.5	6.2	6.2

Table 5. Parameters Used for the Reactions Shown in Figs. 6-12

Reaction	Neutron	Proton
$^{90}Zr(d,p)^{91}Zr$ g.s. d5/2 and 1.2MeV s1/2	Rosen parameters W = 7.5MeV	Rosen parameters W = 4.5MeV
$^{40}Ca(d,p)^{41}Ca$ g.s. f7/2	Rosen parameters	BG parameters W = 3.0MeV, $r_a=r_b=r_c=1.3$fm
$^{40}Ca(d,p)^{41}Ca$ 1.95MeV p3/2 and 3.95MeV p1/2	Rosen parameters $r_a = r_b = r_c = 1.3$fm	Rosen parameters $r_a = r_b = r_c = 1.3$fm W = 4.0MeV
$^{16}O(d,p)^{17}O$ g.s. d5/2	Rosen parameters a=b=c=0.55fm $r_a = r_b = r_c = 1.5$fm W=3.0MeV	Rosen parameters $r_a = r_b = r_c = 1.3$ fm a=b=c=0.55fm W = 3.0MeV
$^{16}O(d,p)^{17}O$ 0.87MeV s1/2	Rosen parameters a=b=c=0.55fm $r_a = r_b = r_c = 1.5$fm W=3.0MeV	Rosen parameters $r_a = r_b = r_c = 1.5$fm a=b=c=0.55fm W = 3.0MeV

Table 6. Data for Reactions Shown in Figs. 6-12

Reaction	Fig.	$d\sigma/d\Omega$	P_D	P_y
$^{16}O(d,p)^{17}O$ 0.87MeV s1/2	6	ref.[100]	ref.[99]	
$^{16}O(d,p)^{17}O$ g.s. d5/2	7	ref.[104]	ref.[99]	
$^{40}Ca(d,p)^{41}Ca$ 3.95MeV p1/2	8	ref.[101]	ref.[102]	ref.[103]
$^{40}Ca(d,p)^{41}Ca$ 1.95MeV p3/2	9	ref.[101]	ref.[102]	ref.[103]
$^{40}Ca(d,p)^{41}Ca$ g.s. f7/2	10	ref.[105]	ref.[102]	squares ref.[103] circles ref.[105]
$^{90}Zr(d,p)^{91}Zr$ 1.2MeV s1/2	11	ref.[98]	ref.[99]	ref.[98]
$^{90}Zr(d,p)^{91}Zr$ g.s. d5/2	12	ref.[98]	ref.[99]	ref.[98]

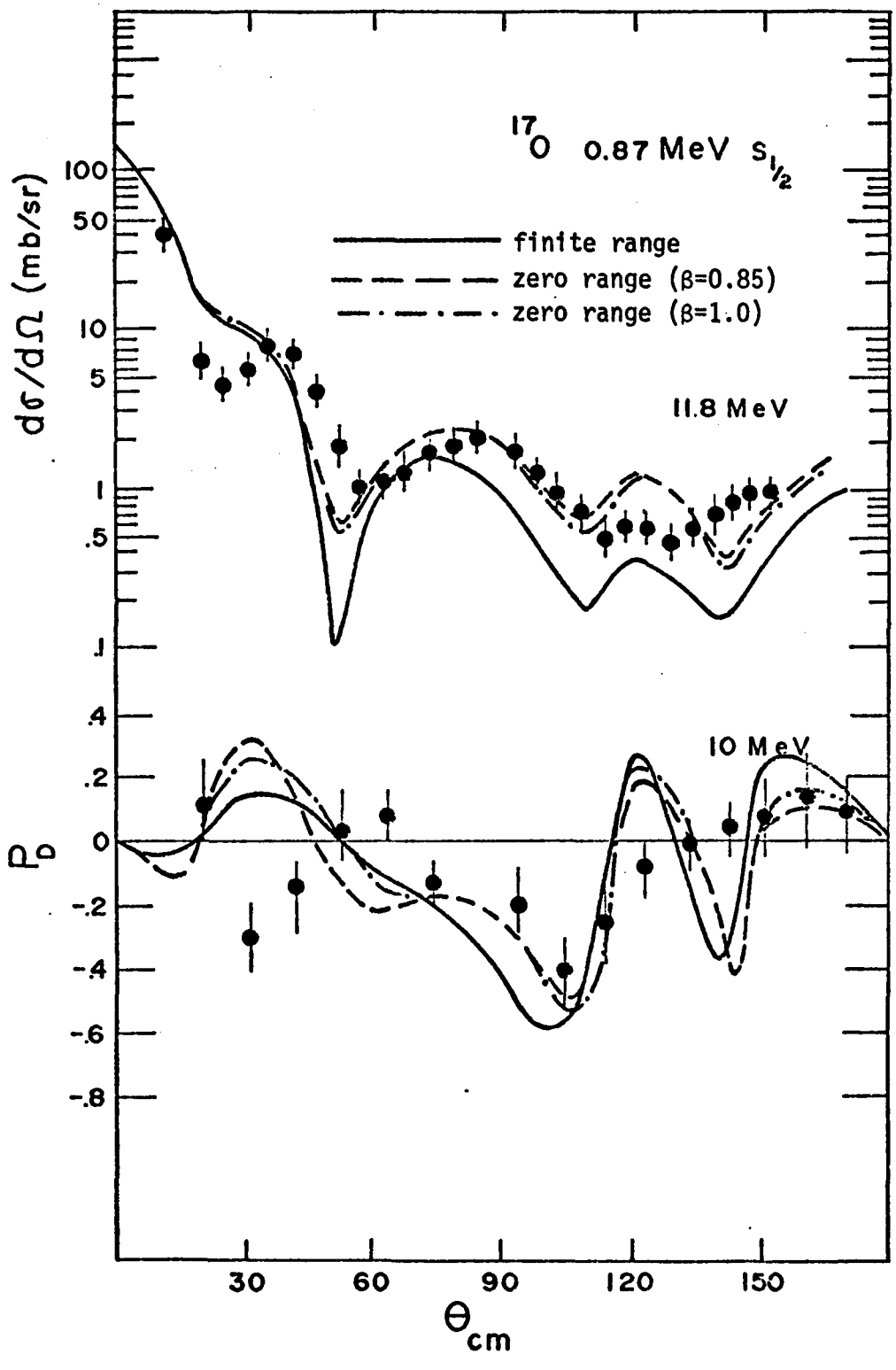

Fig. 6. Finite Range Corrections for the Reaction $^{16}O(d,p)^{17}O$ (0.87MeV $\ell_n = 0$ $j_n = 1/2$)

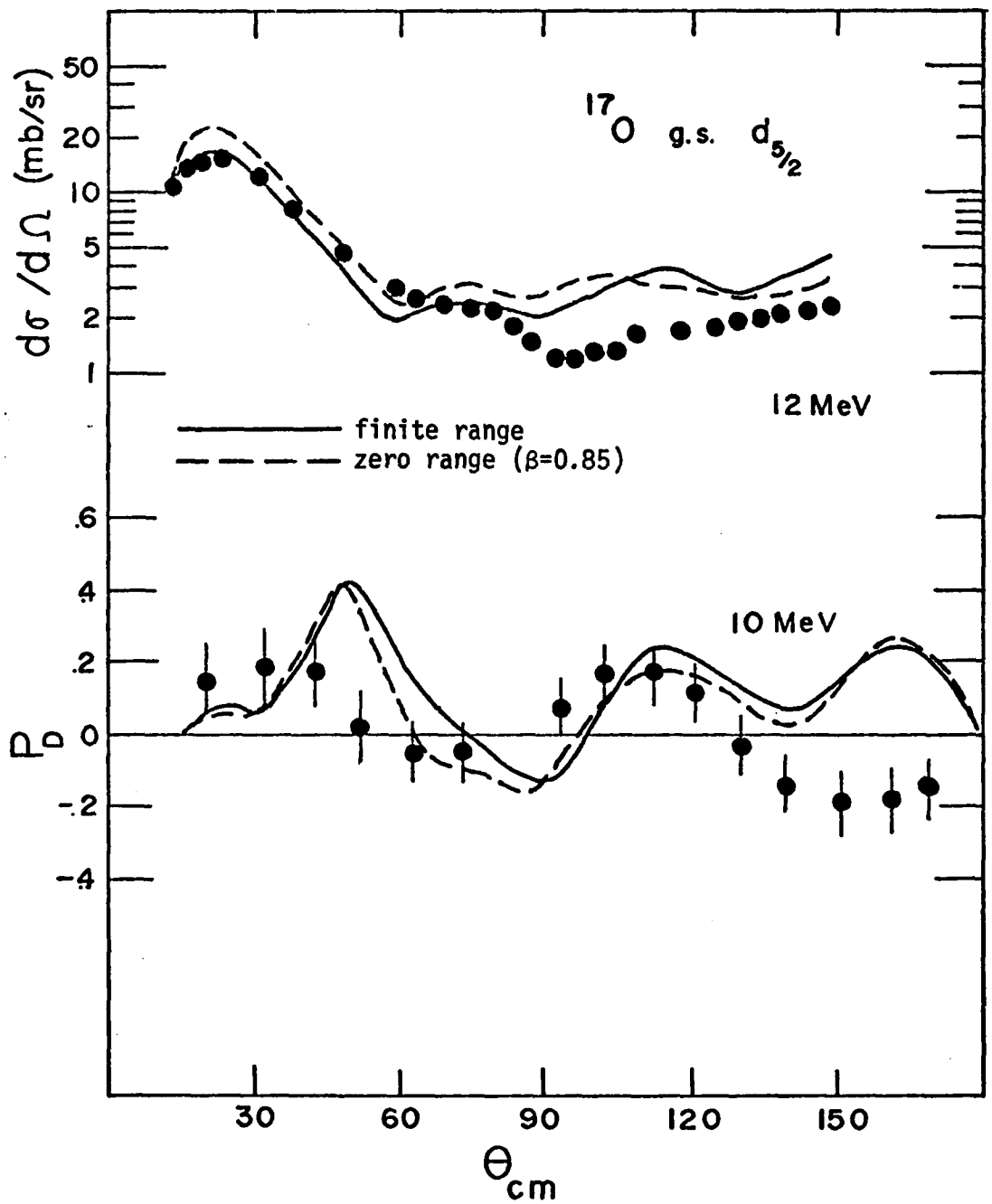

Fig. 7. Finite Range Corrections for the Reaction $^{16}O(d,p)^{17}O$ (g.s. $\ell_n = 2$ $j_n = 5/2$)

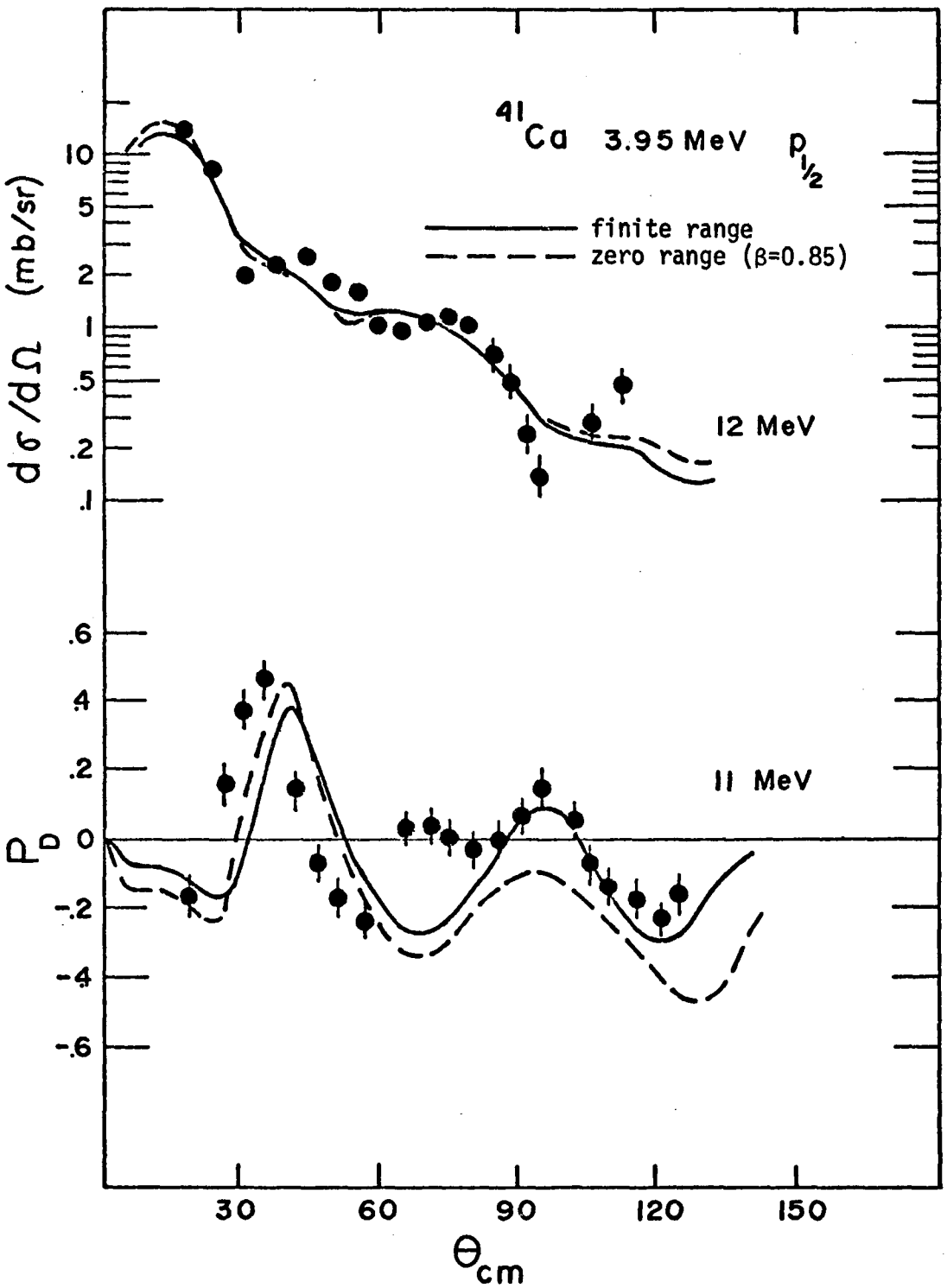

Fig. 8. Finite Range Corrections for the Reaction $^{40}Ca(d,p)^{41}Ca$ (3.95MeV $\ell_n = 1$ $j_n = 1/2$)

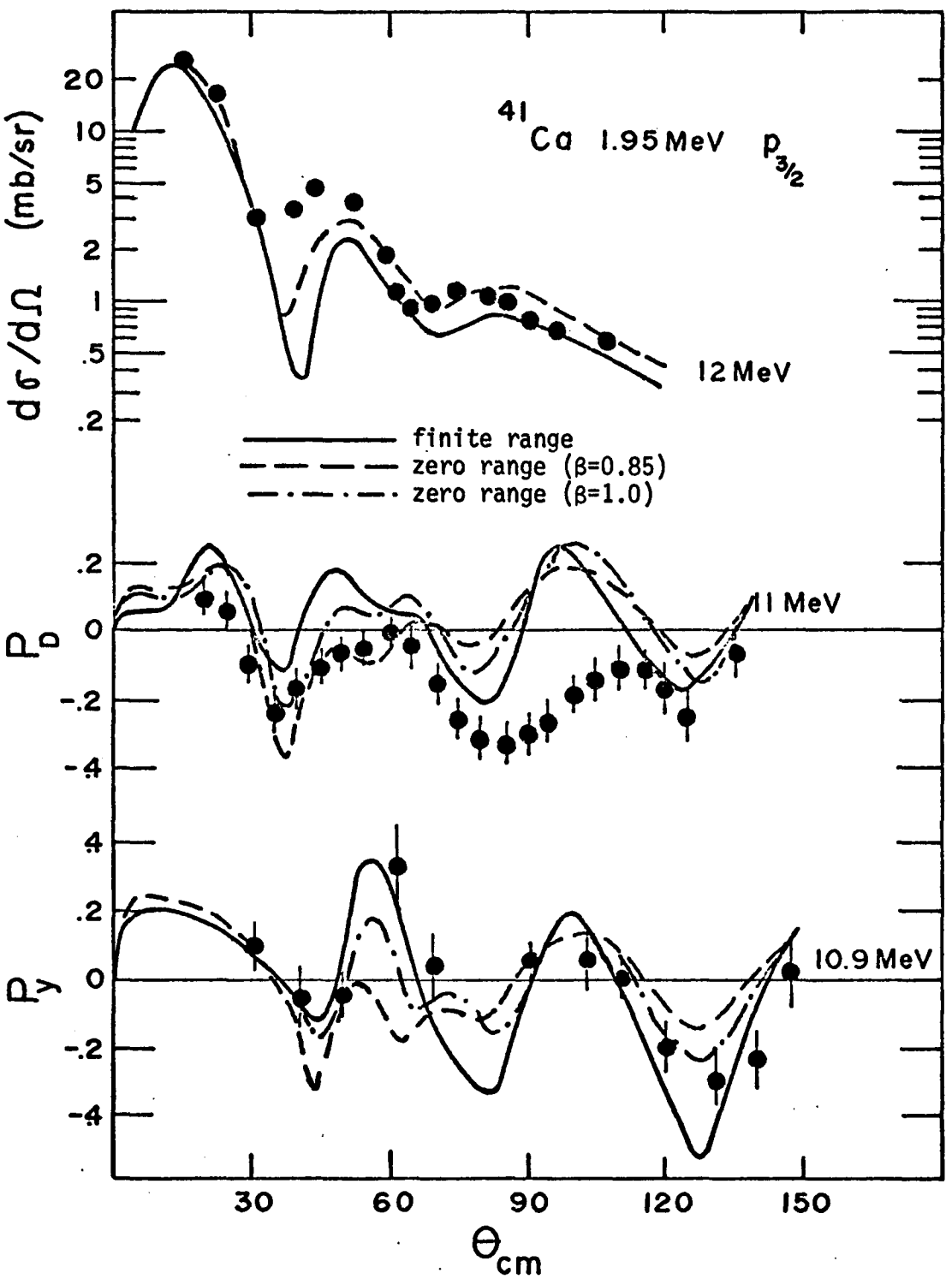

Fig. 9. Finite Range Corrections for the Reaction $^{40}Ca(d,p)^{41}Ca$ (1.95MeV $\ell_n = 1$ $j_n = 3/2$)

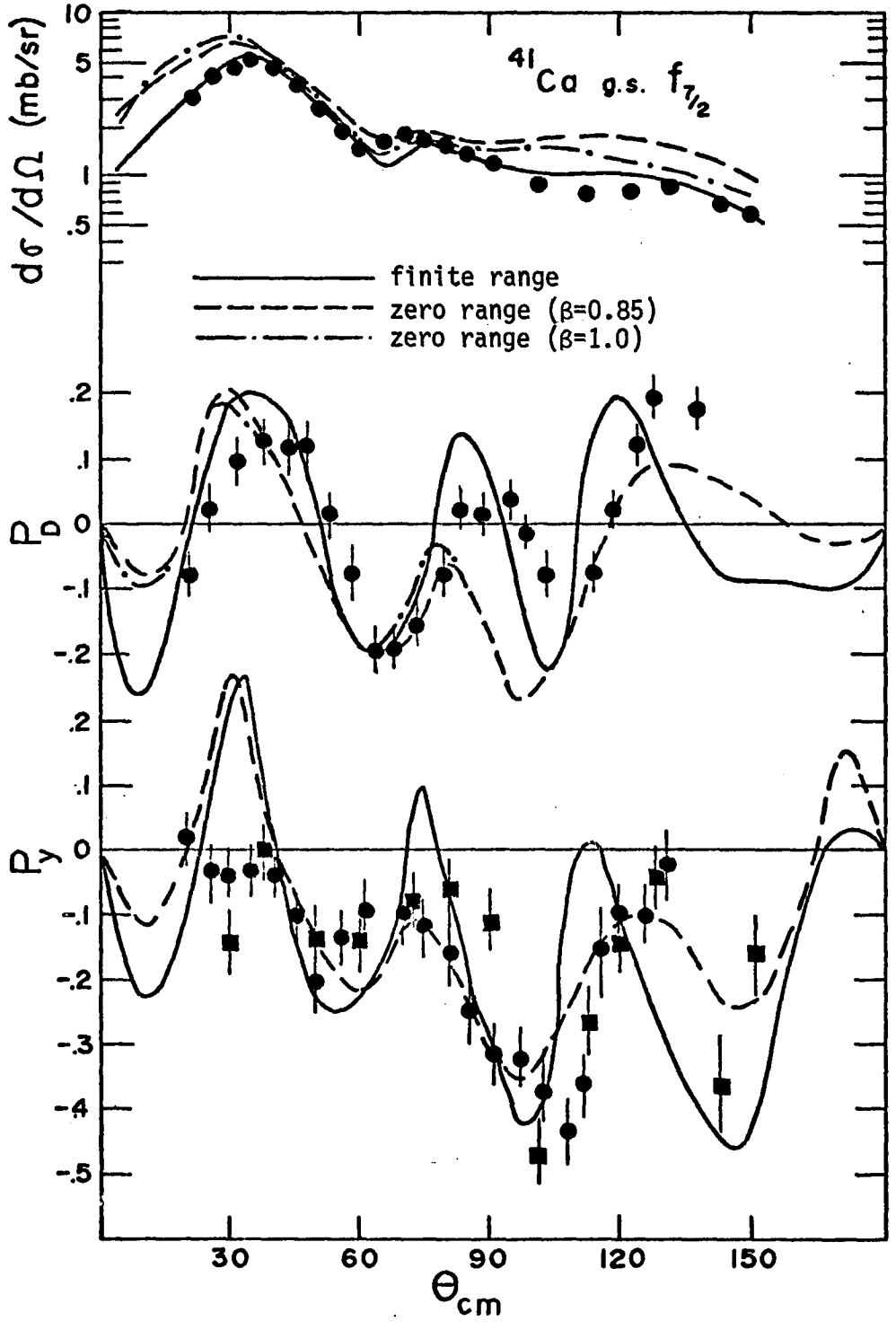

Fig. 10. Finite Range Corrections for the Reaction $^{40}Ca(d,p)^{41}Ca$ (g.s. $\ell_n = 3$ $j_n = 7/2$)

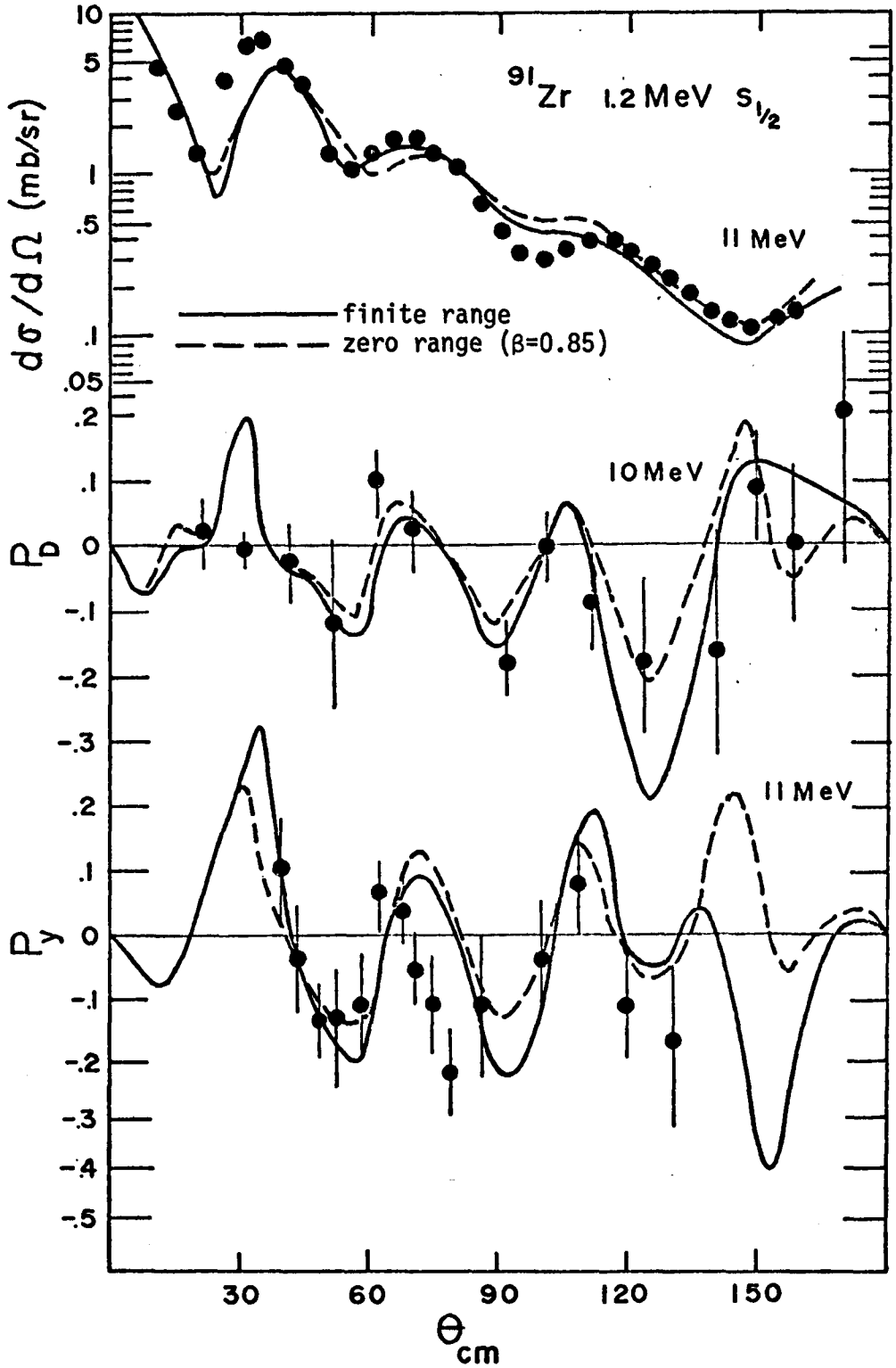

Fig. 11. Finite Range Corrections for the Reaction $^{90}Zr(d,p)^{91}Zr$ (1.2MeV $\ell_n = 0$ $j_n=1/2$)

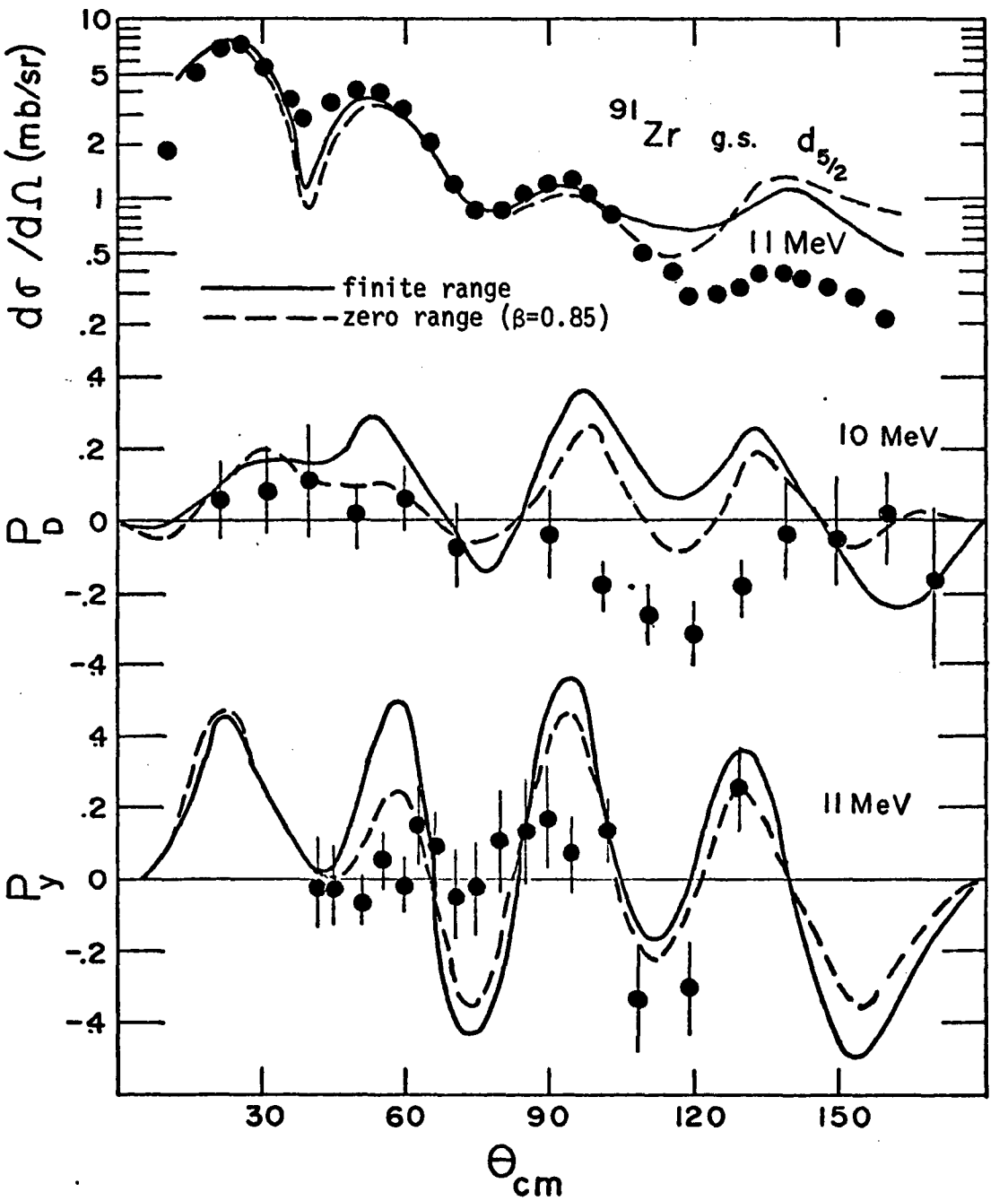

Fig. 12. Finite Range Corrections for the Reaction $^{90}Zr(d,p)^{91}Zr$ (g.s. $\ell_n = 2$ $j_n = 5/2$)

amplitude, the main effect on the integral was to modify the integrand inside the region corresponding to the nuclear interior. In the case of non-locality the local wave function is divided by the factor (109) (see Appendix B for details) which differs most from unity in the nuclear interior. A similar effect is found in the DWBA amplitude. In the approximate method of ref.[83] the main finite range corrections originate from the region of configuration space where the neutron is inside the target nucleus. For example the integrand of the reduced transition amplitude (in ref.[83]) see expression 2.20) is multiplied by a radius-dependent complex factor. Just as for non-locality this factor tends to damp contributions from the nuclear interior.

To see whether the finite range corrections to the WBP model calculations produce a similar damping of the contributions from the nuclear interior the finite range and corresponding zero range calculations were compared with zero range calculations with an increased non-locality β = 1.0 in the factor (109). Some of these comparisons are shown in Figs. 6-12.

The effect of finite range is remarkably similar to that of increased non-locality for the reactions $^{90}Zr(d,p)^{91}Zr$ (1.2 MeV, s1/2), $^{90}Zr(d,p)^{91}Zr$ (g.s. d5/2), $^{40}Ca(d,p)^{41}Ca$ (1.95 MeV, p3/2) and $^{40}Ca(d,p)^{41}Ca$ (3.95 MeV, p1/2). Both tend to reduce the differential cross section at large angles. Both alter P_D and P_y in the same way (e.g. in Fig. 9 note the changes to P_D and P_y near 60 degrees for the reaction leading to the 1.95 MeV state in ^{41}Ca). In these cases where

the finite range effects can be simulated by increasing non-locality the overall finite range corrections are small.

However in certain cases which occur predominantly for target nuclei with $A \lesssim 40$ the finite range effects cannot be simulated by increasing the non-locality. Examples are the reactions $^{16}O(d,p)^{17}O$ (0.87 MeV s1/2) shown in Fig. 6 and $^{40}Ca(d,p)^{41}Ca$ (g.s. f7/2) shown in Fig. 10. Here the corrections to the differential cross section are especially pronounced, the effect increasing with increasing ℓ_n. Both the shape and the magnitude of the cross sections are altered.

In these cases the finite range corrections appear to come from outside as well as inside the target nucleus, with the interior region predominating. Calculations have been made with the finite range corrections only in the region of the neutron configuration space outside a sphere of radius r_n . The results of one such calculation are shown in Fig. 13. The largest effect is shown on the right hand side of Fig. 13 and comes from the nuclear interior $r_n \lesssim 4.5$ fm. Smaller finite range contributions come from the exterior region as seen from the comparison on the left hand side of Fig. 13.

No systematic improvements have been observed in the fits to P_D and P_y from the finite range corrections, even in the cases when the changes are large. In particular the finite range corrections do not remove the discrepancies noted in refs.[60,61]). For example the calculated polarization near 30 degrees in Fig. 10 remains positive over a range of deuteron energies near 11 MeV while the measured values are negative.

Fig. 13. Finite Range Corrections from Various Regions of Neutron Configuration Space

The solid curves represent WBP model calculations for the reaction $^{40}Ca(d,p)^{41}Ca$ (g.s. f7/2) with the zero range approximation on the left and finite range corrections on the right. The broken curves have been calculated with the zero range approximation for $r_n < 4.5$fm and the finite range corrections for larger values of r_n.

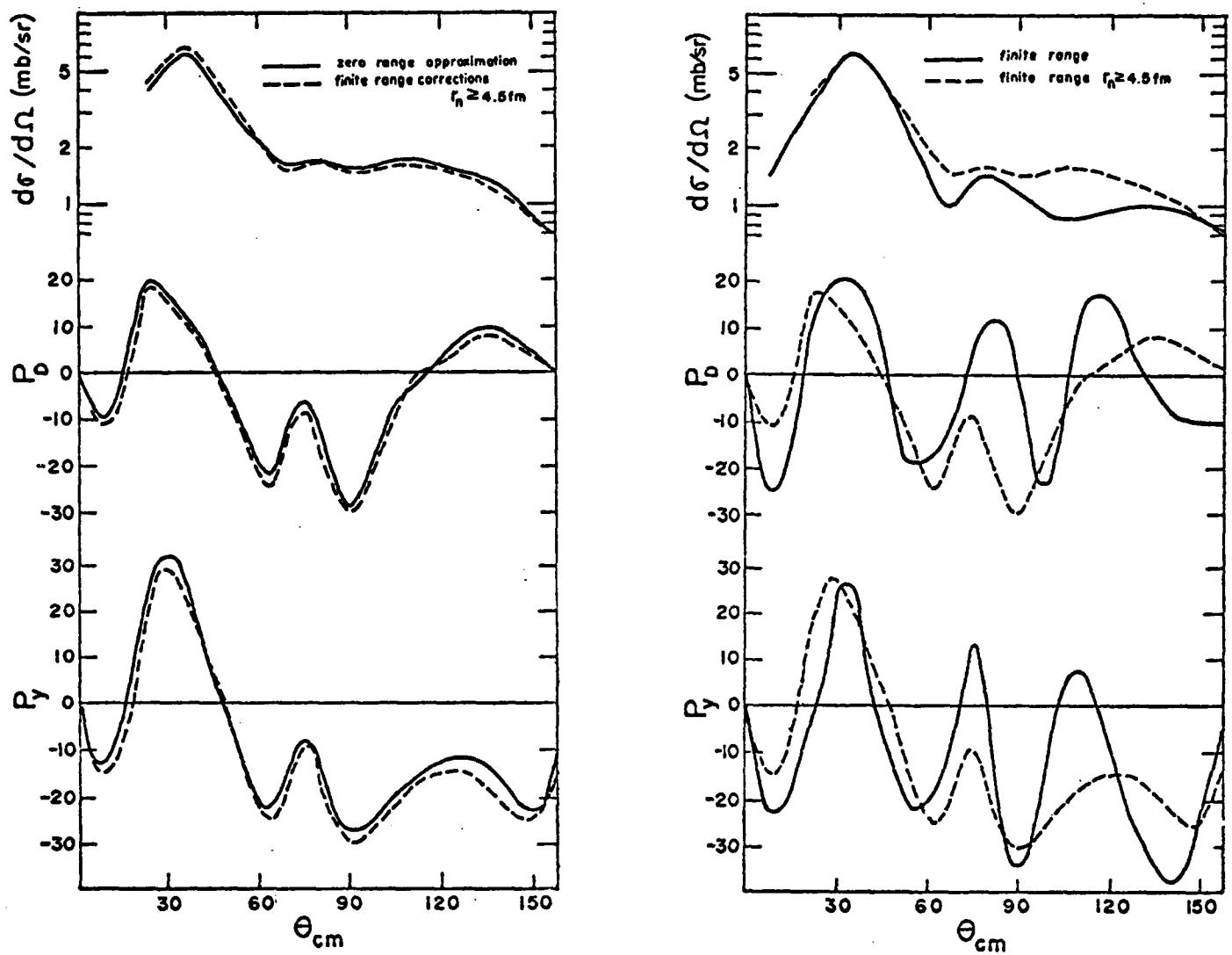

Fig. 13. Finite Range Corrections from Various Regions of Neutron Configuration Space

On the other hand the finite range corrections do systematically change the shape of the calculated differential cross sections by reducing values at large angles relative to the cross section at the stripping peak. In most cases this improves the fits to the experimental data. An example is the reaction $^{40}Ca(d,p)^{41}Ca$ (g.s. f7/2) for which the zero range calculations in ref.[61]) were consistently too large over a wide range of energy for angles greater than 90 degrees.

Quantitative Nature of the Finite Range Corrections

Probably the most important of the finite range effects are the corrections to the magnitude of the differential cross sections and to the spectroscopic factors derived therefrom. There is a systematic trend for the finite range calculations to reduce the magnitude of the cross section at the stripping peak and at large angles.

The reduction in magnitude of $d\sigma/d\Omega$ (with the subscripts ZR and FR referring to zero range and finite range) at the stripping peak is summarized in Table 7. Two trends are apparent. The effect depends both on the orbital angular momentum transfer ℓ_n and on the size of the target nucleus. For reactions with the same value of ℓ_n the reduction is stronger for small nuclei. For reactions on the same target nucleus (see $^{40}Ca(d,p)^{41}Ca$ and $^{16}O(d,p)^{17}O$) the reduction increases with ℓ_n. This effect is independent of the values for Q and j_n for the reaction.

Although the peak value of the calculated cross section is very important, the entire angular distribution is actually used to extract the spectroscopic factor. The back-angle distributions usually carry less weight due to uncertainty from the small magnitudes involved and

Table 7. Depression of Cross Section at the Stripping Peak

Reaction	$R \equiv (d\sigma/d\Omega)_{FR}/(d\sigma/d\Omega)_{ZR}$	$100(1 - R)$
$^{16}O(d,p)^{17}O$ 0.87MeV s1/2*	0.83	17%
$^{16}O(d,p)^{17}O$ g.s. d5/2	0.76	24%
$^{40}Ca(d,p)^{41}Ca$ 3.95MeV p1/2	0.95	5%
$^{40}Ca(d,p)^{41}Ca$ 1.95MeV p3/2	0.89	11%
$^{40}Ca(d,p)^{41}Ca$ g.s. f7/2	0.72	28%
$^{90}Zr(d,p)^{91}Zr$ 1.2MeV s1/2*	0.97	3%
$^{90}Zr(d,p)^{91}Zr$ g.s. d5/2	1.02	-2%

*Measured at the second maximum for reactions with $\ell_n = 0$

possible compound nucleus contributions (usually small and isotropic). For the examples discussed, however, these problems are not expected to be serious. Spectroscopic factors with and without finite range corrections have been extracted by comparing data and calculations visually on logarithmic plots. This method has proven consistent with automatic search routines based upon a chi-squared minimization[106]). Table 8 shows the extracted spectroscopic factors along with the percentage increase over the spectroscopic factors extracted using the zero range calculation.

Summary and Discussion

We have shown that it is possible to make accurate finite range WBP model calculations using the configuration space expansion of the integral (60). For an appropriate choice of the form of the potential V_{np} the expansion has been shown to converge to a value which depends very weakly on the shape of V_{np} . This can be contrasted to similar attempts to include finite range effects in DWBA calculations, where the corresponding expansion has not converged, and shape independence has not been demonstrated.

The finite range corrections shown in Figs. 6-12 do not change the major qualitative nature of the predicted values for P_D, P_y and $d\sigma/d\Omega$. However they are comparable in magnitude to the contributions from the deuteron D-state and to the uncertainties which arise in the WBP model calculations from ambiguity in the optical potential parameters. For quantitative comparison of the WBP model with experiment it is necessary to include them.

Table 8. Comparison of Spectroscopic Factors

Reaction	Zero Range	Finite Range	% increase
$^{16}O(d,p)^{17}O$ 0.87MeV s1/2	0.65	0.80	23%
$^{16}O(d,p)^{17}O$ g.s. d5/2	0.52	0.63	21%
$^{40}Ca(d,p)^{41}Ca$ 3.95MeV p1/2	0.71	0.77	8%
$^{40}Ca(d,p)^{41}Ca$ 1.95MeV p3/2	0.73	0.82	12%
$^{40}Ca(d,p)^{41}Ca$ g.s. f7/2	0.57	0.71	25%
$^{90}Zr(d,p)^{91}Zr$ 1.2MeV s1/2	0.97	0.93	-4%
$^{90}Zr(d,p)^{91}Zr$ g.s. d5/2	0.90	0.91	1%

APPENDIX A

INTEGRATION OF EQUATION (64) BY FOURIER TRANSFORMS

The integral

$$I \equiv \int s^2 ds \int d\Omega_s \, D(s) \, e^{\vec{s}\cdot\vec{\nabla}_n} J(\vec{r}_n) \qquad \text{(A1)}$$

poses a difficulty in the interpretation of the operator $\vec{\nabla}_n$. It will be shown in this appendix that $\vec{\nabla}_n$ may be treated as if it were an algebraic quantity so that the integration over Ω_s in Eq. (A1) can be carried out. The result is

$$I = 4\pi \int s^2 ds \, D(s) \, \frac{\sinh(s|\nabla_n|)}{s|\nabla_n|} \, J(\vec{r}_n). \qquad \text{(A2)}$$

The interpretation of the operator $\vec{\nabla}_n$ is made clear by introducing the Fourier transform of the function $J(\vec{r}_n)$. The term $\exp(\vec{s}\cdot\vec{\nabla}_n)$ in Eq. (A1) will be seen to operate only on a simple exponential term so the desired integration over Ω_s can easily be completed. The operator $\vec{\nabla}_n$ and the inverse Fourier transform are then reintroduced to achieve the result (A2). Details are given below.

Inserting the Fourier transform

$$J(\vec{r}_n) = \int d\vec{k}_n \exp(i\vec{k}_n\cdot\vec{r}_n)\,\tilde{J}(\vec{k}_n) \qquad \text{(A3)}$$

in Eq. (A1) and reversing the order of integration yields

$$I = \int d\vec{s}\, D(s) \int d\vec{k}_n \exp(\vec{s}\cdot\vec{\nabla}_n)\exp(i\vec{k}_n\cdot\vec{r}_n)\,\tilde{J}(\vec{k}_n). \qquad \text{(A4)}$$

The operator $\exp(\vec{s}\cdot\vec{\nabla}_n)$ now acts only on the term $\exp(i\vec{k}_n\cdot\vec{r}_n)$. Since $\vec{s}$ is not operated on by $\vec{\nabla}_n$, the relation

$$(\vec{s}\cdot\vec{\nabla}_n)\exp(i\vec{k}_n\cdot\vec{r}_n) = (i\vec{k}_n\cdot\vec{s})\exp(i\vec{k}_n\cdot\vec{r}_n) \tag{A5}$$

follows. Taken j times, the operation in (A5) gives the expression

$$(\vec{s}\cdot\vec{\nabla}_n)^j \exp(i\vec{k}_n\cdot\vec{r}_n) = (i\vec{k}_n\cdot\vec{s})^j \exp(i\vec{k}_n\cdot\vec{r}_n) \tag{A6}$$

from which follows the result

$$\begin{aligned}\exp(\vec{s}\cdot\vec{\nabla}_n)\exp(i\vec{k}_n\cdot\vec{r}_n) &= \left[1+\vec{s}\cdot\vec{\nabla}_n + \frac{(\vec{s}\cdot\vec{\nabla}_n)^2}{2!}+\dots\right]\exp(i\vec{k}_n\cdot\vec{r}_n)\\ &= \left[1+i\vec{k}_n\cdot\vec{s}+(i\vec{k}_n\cdot\vec{s})^2+\dots\right]\exp(i\vec{k}_n\cdot\vec{r}_n)\\ &= \exp(i\vec{k}_n\cdot\vec{s})\exp(i\vec{k}_n\cdot\vec{r}_n)\cdot\end{aligned} \tag{A7}$$

The angular integration over Ω_s can now be easily performed. Inserting the expression (A7) into the integral (A4) yields

$$I = \int d\vec{k}_n\, \tilde{J}(\vec{k}_n)\, \vartheta \exp(i\vec{k}_n\cdot\vec{r}_n) \tag{A8}$$

where the expression

$$\vartheta \equiv \int s^2 ds \int d\Omega_s\, D(s) \exp(i\vec{k}_n\cdot\vec{s}) \tag{A9}$$

contains the desired angular integral. Since $\vec{s}$ is a dummy variable and $D(s)$ is isotropic, the $\hat{z}$ axis is taken parallel to $\vec{k}_n$. The result of the integration over Ω_s is

$$\vartheta = 4\pi \int s^2 ds\, D(s)\, \frac{\sin(k_n s)}{k_n s}\,. \tag{A10}$$

The operator $\vec{\nabla}_n$ can be reintroduced by using the expansion

$$\frac{\sin(k_n s)}{k_n s} = \frac{\exp(ik_n s) - \exp(-ik_n s)}{2ik_n s}$$

$$= 1 + \frac{(ik_n s)^2}{3!} + \frac{[(ik_n s)^2]^2}{5!} + \cdots \quad . \tag{A11}$$

Since $\vec{\nabla}_n$ is independent of $\vec{k}_n$ and $\vec{s}$, the relation

$$(ik_n s)^2 \exp(i\vec{k}_n \cdot \vec{r}_n) = s^2 \nabla_n^2 \exp(i\vec{k}_n \cdot \vec{r}_n) \tag{A12}$$

follows, which applied j times gives the result

$$(ik_n s)^{2j} \exp(i\vec{k}_n \cdot \vec{r}_n) = (s|\nabla_n|)^{2j} \exp(i\vec{k}_n \cdot \vec{r}_n) \quad . \tag{A13}$$

Combining expressions (A11) and (A13) gives the relation

$$\frac{\sin(k_n s)}{k_n s} \exp(i\vec{k}_n \cdot \vec{r}_n) = \left[1 + \frac{(s|\nabla_n|)}{3!} + \ldots\right] \exp(i\vec{k}_n \cdot \vec{r}_n)$$

$$= \frac{\sinh(s|\nabla_n|)}{s|\nabla_n|} \exp(i\vec{k}_n \cdot \vec{r}_n) \quad . \tag{A14}$$

Finally, combining the expressions (A8), (A10), and (A14), and interchanging the order of integration yields the integral

$$I = 4\pi \int s^2 ds\, D(s) \frac{\sinh(s|\nabla_n|)}{s|\nabla_n|} \int d\vec{k}_n \exp(i\vec{k}_n \cdot \vec{r}_n) \tilde{J}(\vec{k}_n) \quad . \tag{A15}$$

The last integration on the right hand side of Eq. (A15) is the Fourier transform of $J(\vec{r}_n)$ so Eq. (A15) reduces to the integral

$$I = 4\pi \int s^2 ds\, D(s) \frac{\sinh(s|\nabla_n|)}{s|\nabla_n|} J(\vec{r}_n) \qquad \text{(A16)}$$

which is identical with Eq. (A2), the desired result.

APPENDIX B

PREVIOUS APPLICATION OF EXPANSION METHODS

In this appendix the use of expansion methods in calculating non-local wave functions and finite range effects in the DWBA is discussed.

Approximate Solution of the Non-Local Schroedinger Equation

The Schroedinger equation with a non-local potential may be written[76]

$$-\frac{\hbar^2}{2m}\nabla^2\psi_N(\vec{r}) + I = E\psi_N(\vec{r}) \tag{B1}$$

where

$$I = \int d\vec{s}\,\delta_\beta(s)\,U_N(\vec{r}+\tfrac{1}{2}\vec{s})\psi_N(\vec{r}+\vec{s}) \tag{B2}$$

and δ_β is usually taken to be of Gaussian form

$$\delta_\beta(s) = (\pi^{3/2}\beta^3)^{-1}\exp(-s^2/\beta^2) \tag{B3}$$

The integral (B2) is of the form (61) where we identify $D(s)$ with $\delta_\beta(s)$ and J with the remaining product

$$J = U_N(\vec{r}+\tfrac{1}{2}\vec{s})\psi_N(\vec{r}+\vec{s}) \tag{B4}$$

It is most convenient to use the momentum space method to evaluate the integral since the configuration space method leads immediately

to the cross product difficulty discussed in Chapter 4. If the derivatives of the potential $U_N(\vec{r})$ are neglected, the momentum space expansion (78) applied to the integral (B2) gives

$$I = G(\alpha^2)\, U_N(\vec{r})\psi_N(\vec{r}) + G'(\alpha^2)\, U_N(\vec{r})(\nabla_r^2 - \alpha^2)\psi_N(\vec{r}) \tag{B5}$$

where

$$G(\alpha^2) = \int d\vec{s}\; \delta_\rho(s) \exp(i\vec{\alpha}\cdot\vec{s}) \; . \tag{B6}$$

The second term in Eq. (B5) vanishes when

$$\alpha^2 = \frac{\nabla^2 \psi_N(\vec{r})}{\psi_N(\vec{r})} \; . \tag{B7}$$

A convenient approximation to this value of α^2 is given by the semiclassical value associated with the kinetic energy in a local potential (hence the name Local Energy Approximation or "LEA")

$$\alpha^2 = \frac{2m}{\hbar^2}\left[E - U_L(\vec{r})\right] \tag{B8}$$

where the local potential $U_L(\vec{r})$ is related to $U_N(\vec{r})$ by

$$U_L(\vec{r}) = G(\alpha^2)\, U_N(\vec{r}) \; . \tag{B9}$$

It should be noted that this prescription for α^2 which is responsible for the success of the momentum space expansion in this case requires that the function J in the integral (B4) have the form

$$J(\vec{r}_n + \vec{s}) \propto \psi_N(\vec{r}_n + \vec{s})$$

where ψ_N is an approximate solution of a local Schroedinger equation.

With this value of α^2 the solution to the non-local Schroedinger equation (B1) can be written in terms of the solution of a local Schroedinger equation

$$\Psi_N(\vec{r}) = \Psi_L(\vec{r})/f(\vec{r}) \tag{B10}$$

where the form of the function $f(\vec{r})$ can be determined. The equation (B1) becomes[76] with $g = 2mG/\hbar^2$

$$\left\{-(\nabla^2+\frac{2mE}{\hbar^2}) - \frac{2(\vec{\nabla}f)^2}{f^2} + \frac{\nabla^2 f}{f} + gU_N - g'(1+g'U_N)^{-1}\left[\frac{1}{4}\nabla^2 U_N - \frac{\vec{\nabla}f\cdot\vec{\nabla}U_N}{f}\right]\right\}\Psi_L$$
$$= \left[(1+g'U_N)^{-1}\left(g'\vec{\nabla}U_N - \frac{2\vec{\nabla}f}{f}\right]\cdot\vec{\nabla}\Psi_L \right. . \tag{B11}$$

The right hand side of Eq. (B11) will vanish if f is chosen to satisfy

$$\frac{\vec{\nabla}f}{f} = \frac{1}{2}g'(1+g'U_N)^{-1}\vec{\nabla}U_N \quad . \tag{B12}$$

For this choice of f Eq. (B11) becomes a local Schroedinger equation

$$-(\nabla^2+\frac{2mE}{\hbar^2})\Psi_L + \left[gU_N + \frac{1}{4}(1+g'U_N)^{-2}\left\{(1+g'U_N)g'\nabla^2U_N - (g'\nabla U_N)^2\right\}\right]\Psi_L = 0 \quad . \tag{B13}$$

Since $g'(\alpha^2)$ is independent of $\vec{r}$ except in the surface region, one can set the term g' = constant to integrate Eq. (B12) with the result

$$f(\vec{r}) = \left[1 + g'U_N\right]^{1/2} \tag{B14}$$

which for the Gaussian form (B3) becomes

$$f(\vec{r}) = \left[1 - \frac{m\beta^2}{2\hbar^2}U_L(\vec{r})\right]^{1/2} \quad . \tag{B15}$$

In calculating the WBP model amplitude the non-local nucleon-nucleus wave functions are calculated by solving the local Schroedinger equation (B13) and dividing by the factor (B15).

Expansion Methods for Finite Range DWBA Calculations

The DWBA transition amplitude contains the integral[82])

$$I = \int d\vec{r}_n \, \psi_n(\vec{r}_n) \int d\vec{s} \, D(s) \psi_p(\vec{r}_n + \vec{s}) \psi_d(\vec{r}_n + \tfrac{1}{2}\vec{s}) \qquad \text{(B16)}$$

which has the same form as expression (61) with $D(s) = V_{np}(s)\phi_d(s)$ where ϕ_d is the internal deuteron wave function, and

$$J = \psi_d(\vec{r}_n + \tfrac{1}{2}\vec{s}) \, \psi_p(\vec{r}_n + \vec{s}) \qquad \text{(B17)}$$

where ψ_p and ψ_d are the distorted waves for the proton and deuteron. The configuration space expansion for evaluating I (which is usually referred to[65]) as the "effective mass approximation" (EMA)) leads immediately to the cross product difficulty. With the expansion (69) the integral (B16) becomes

$$I = \int d\vec{r}_n \, \psi_n(\vec{r}_n) \left\{ \int d\vec{s} \, D(s) \psi_p(\vec{r}_n) \psi_d(\vec{r}_n) + \tfrac{1}{6} \int d\vec{s}\, s^2 D(s) \left[\tfrac{1}{2}\vec{\nabla}_1 + \vec{\nabla}_2\right]^2 \psi_p(\vec{r}_n) \psi_d(\vec{r}_n) + \cdots \right\} \qquad \text{(B18)}$$

where $\vec{\nabla}_1$ acts only on ψ_d and $\vec{\nabla}_2$ acts only on ψ_p. For the first order term in expression (B18) the cross product difficulty can be overcome. By defining an operator $\vec{\nabla}$ acting on both ψ_p and ψ_d one can write

$$\left(\tfrac{1}{2}\vec{\nabla}_1 + \vec{\nabla}_2\right)^2 \psi_p(\vec{r}_n) \psi_d(\vec{r}_n) = \left(\tfrac{1}{2}\nabla^2 + \tfrac{1}{2}\nabla_2^2 - \tfrac{1}{4}\nabla_1^2\right) \psi_p(\vec{r}_n) \psi_d(\vec{r}_n) \quad . \qquad \text{(B19)}$$

The Schroedinger equations for ψ_d and ψ_p can be used to evaluate $\nabla_1^2\psi_d$ and $\nabla_2^2\psi_p$. The effect of ∇^2 on the first order term in the expansion (B18) can be evaluated by applying Green's theorem

$$\int d\vec{r}_n\, \psi_n(\vec{r}_n)\nabla^2[\psi_p(\vec{r}_n)\psi_d(\vec{r}_n)] = \int d\vec{r}_n\, [\nabla^2\psi_n(\vec{r}_n)]\psi_p(\vec{r}_n)\psi_d(\vec{r}_n) \qquad \text{(B20)}$$

and using the Schroedinger equation for the neutron wave function ψ_n to evaluate $\nabla^2\psi_n$. The second and higher order terms in the expansion (B18) are much more difficult to evaluate because they contain terms $(\vec{\nabla}_1\cdot\vec{\nabla}_2)^m$ of order $m>1$. No attempt has been made in the literature to carry the EMA expansion for this application beyond second order.

The momentum space expansion which is referred to[70]) as the "local energy approximation" (LEA) has both the cross product difficulty and the evaluation of α^2 problem. Because the function J is a product of two wave functions and is not a solution of a Schroedinger equation as in the non-locality problem, the evaluation of α^2 problem cannot be overcome. The momentum space expansion (78) applied to the integral (B16) gives

$$I = \int d\vec{r}_n \left\{ \tilde{D}(\alpha^2)\psi_p(\vec{r}_n)\psi_d(\vec{r}_n) - \tilde{D}'(\alpha^2)(\nabla_s^2+\alpha^2)\left[\psi_p(\vec{r}_n+\vec{s})\psi_d(\vec{r}_n+\tfrac{1}{2}\vec{s})\right]_{s=0} + \cdots \right\} . \qquad \text{(B21)}$$

After some manipulations and use of the Schroedinger equation, one can show that the second term of the expansion (B21) vanishes for

$$\alpha^2(\vec{r}_n) = \tfrac{1}{2}K_p^2(\vec{r}_n) - \tfrac{1}{4}K_d^2(\vec{r}_n) - \frac{\nabla^2[\psi_p(\vec{r}_n)\psi_d(\vec{r}_n)]}{\psi_p(\vec{r}_n)\psi_d(\vec{r}_n)} \qquad \text{(B22)}$$

where $\hbar^2 K_p^2/2m_p$, $\hbar^2 K_d^2/2m_d$ are the proton and deuteron energies. Thus α^2 is a complicated function of $\vec{r}_n$. Since α^2 should be the value of K^2 corresponding to the peak of the Fourier transform of $\psi_p \psi_d$, and since $\psi_p \psi_d$ is a complicated function it is not surprising that α^2 is difficult to find. For this reason all efforts to apply this method to finite range DWBA calculations have proven unsuccessful[81]).

APPENDIX C

BEHAVIOR OF THE EXPANSION COEFFICIENTS $b_L(r_n)$ NEAR THE ORIGIN

The coefficients $b_L(r_n)$ in expression (97) of Chapter 4 are derived from the zero range coefficients

$$a_L(r_n) \propto \sum_{\ell\ell'} a_{\ell\ell'} \left| \langle \ell\, 0\ \ell'\, 0 \mid L\, 0 \rangle \right|^2 \chi_\ell(r_n) \chi^*_{\ell'}(r_n) \quad . \tag{C1}$$

The partial waves $\chi_\ell(r_n)$ are generated from a complex optical potential which approaches a constant complex value V_0 as $r_n \to 0$. Near the origin the radial function u_ℓ defined by $u_\ell \equiv \rho \chi_\ell$ obeys

$$\frac{\partial^2 u_\ell(\rho)}{\partial \rho^2} + \left[1 + V_0 - \frac{\ell(\ell+1)}{\rho^2} \right] u_\ell(\rho) = 0 \quad , \qquad \begin{aligned} \rho &= k r_n \\ \frac{\hbar^2 k^2}{2\mu} &= E \end{aligned} \tag{C2}$$

If $u_\ell(\rho)$ is expanded in a power series

$$u_\ell(\rho) = \rho^{\ell+1} \left[1 + c_1 \rho + c_2 \rho^2 + \cdots \right] \tag{C3}$$

and inserted in Eq. (C2) one has after setting the coefficients of each power of ρ^ℓ equal to zero separately

$$c_j = 0 \qquad\qquad j = \text{odd}$$

$$c_j = -\frac{(1 + V_0)}{j(2\ell + 1 + j)} c_{j-2} \qquad j = \text{even} \quad . \tag{C4}$$

Thus for small r_n the partial wave $\chi_\ell(r_n)$ contains only even powers of r_n

$$\chi_\ell(r_n) \propto r_n^\ell \sum_{m=0} d_m r_n^{2m} \tag{C5}$$

where the coefficients d_m are related to the coefficients C_{2m} in Eq. (C3) by $d_m = C_{2m} k^{2m}$.

The behavior of the coefficients a_L near the origin can now be determined. Combining the expressions (C1) and (C5) gives

$$a_L(r_n) \propto \sum_{\ell,\ell',m,m'} a_{\ell\ell'} |\langle \ell 0 \ell' 0 | L 0\rangle|^2 r_n^{\ell+\ell'} d_m d_{m'}^* r_n^{2(m+m')} . \tag{C6}$$

The vector coupling coefficient $\langle \ell 0 \ell' 0 | L 0\rangle$ requires $(\ell+\ell'-L)$ to be even and non-negative so the lowest power of $\rho^{\ell+\ell'}$ is ρ^L. Rearranging terms in the $\sum_{m,m'}$ one can write

$$\begin{aligned} a_L(r_n) \propto r_n^L \sum_{m,m'} d_m d_{m'}^* r_n^{2(m+m')} &= r_n^L \{ |d_0|^2 + (d_0 d_1^* + d_1 d_0^*) r_n^2 + \\ &\quad + (|d_1|^2 + d_0 d_2^* + d_2 d_0^*) r_n^4 + \cdots \} \\ &= r_n^L \{ |d_0|^2 + 2\,\mathrm{Re}(d_0 d_1^*) r_n^2 + [|d_1|^2 + 2\,\mathrm{Re}(d_0 d_2^*)] r_n^4 + \cdots \} \\ &= r_n^L \sum_{m=0} B_m r_n^{2m} . \end{aligned} \tag{C7}$$

Note the B_m are real as required since the $a_L(r_n)$ are expansion coefficients of $|\chi_\ell(r_n)|$ and that the expansion (C7) for the a_L has exactly the same form as the expression (C5) for the $\chi_\ell(r_n)$.

One can now determine the behavior of the coefficients $b_L(r_n)$ near the origin by inserting the result (C7) for $r_n a_L(r_n)$ into the generating equation (97) for the coefficients $b_L(r_n)$. Applying the operator $\left[D_n^2 - \frac{L(L+1)}{r_n^2} \right]$ p times to $r_n a_L(r_n)$ as given by the expansion (C7) yields the result where $D_n^2 = \partial^2/\partial r_n^2$

$$\frac{1}{r_n}\left[D_n^2 - \frac{L(L+1)}{r_n^2} \right]^p \left[r_n a_L(r_n) \right] = \sum_{m=p} B_m 2^p (m-p+1)(m-p+2)\cdots(m) \times$$
$$\times (2m+2L+1-2p+2)(2m+2L+1-2p+4) \times$$
$$\times (2m+2L+1-2p+6)\cdots(2m+2L+1) \times$$
$$\times r_n^{2m+L-2p} . \qquad \text{(C8)}$$

The summation (C8) begins at $m = p$ due to differentiation of constant terms so that the lowest power of r_n in the summation (C8) is r_n^L. Hence near the origin the coefficients

$$b_L(r_n) = \sum_{p=0}^{\infty} \frac{\bar{s}^{2p}}{(2p+1)!} \frac{1}{r_n}\left[D_n^2 - \frac{L(L+1)}{r_n^2} \right]^p \left[r_n a_L(r_n) \right] \qquad \text{(C9)}$$

are regular for all L.

APPENDIX D

NUMERICAL DIFFERENTIATION METHODS

Accurate finite range corrections in the WBP model rely upon the generation of accurate coefficients $\ell_L(r_n)$ given in expression (97) of Chapter 4. Evaluation of the term $\left[D_n^2 - \frac{L(L+1)}{r_n^2} \right]^m \left[r_n \, a_L(r_n) \right]$ requires a numerical differentiation routine capable of computing accurate even-order derivatives. Typically the functions $r_n a_L(r_n)$ are computed for eighty equally spaced values of r_n from 0 to 16 fm, giving a step length h = 0.2 fm. Since the accuracy of many differentiation algorithms is sensitive to the step length and since it would be very costly to decrease the step length, an algorithm was sought which would give satisfactory accuracy for the step length used in the existing zero range code.

Because the analytical study of errors inherent in numerical methods is not very revealing it was thought necessary to test various methods by using them to compute even derivatives of an analytical function with known derivatives. Since the functions $r_n a_L(r_n)$ are oscillatory functions it was decided to test the methods with sine curves of variable frequency. For this situation one can not only study roundoff error by increasing the "word" size (double precision arithmetic) used in the computer but also study directly the accuracy as a function of step length.

Among the methods tested were a seven point central difference formula based on Stirling's interpolating polynomial and a Lagrangian interpolation formula written for either three or five points.

The central difference formula is given by twice differentiating Stirling's interpolating polynomial[107]). Denoting the seven equally spaced functional values by y_{i-3}, y_{i-2}, ..., y_{i+3} the second derivative at the point x_i is

$$\ddot{y}_i = \frac{1}{h^2}\left[\frac{1}{90}(y_{i+3}+y_{i-3}) - \frac{3}{20}(y_{i+2}+y_{i-2}) + \frac{3}{2}(y_{i+1}+y_{i-1}) - \frac{49}{180}y_i\right] . \qquad \text{(D1)}$$

Since the formula (D1) is not applicable for the first three and last three points, Newton's forward formula[107]) which, including six terms, twice differentiated reads for the first three points

$$\ddot{y}_i = \frac{1}{h^2}\left[\frac{15}{4}y_i - \frac{77}{6}y_{i+1} + \frac{107}{6}y_{i+2} - 13y_{i+3} + \frac{61}{12}y_{i+4} - \frac{5}{6}y_{i+5}\right] \qquad \text{(D2)}$$

(If there are n points, one puts $y_i \to -y_{n-i}$ in Eq. (D2) for the last three points).

The other methods take the first derivative of Lagrange's interpolating polynomial of degree 2 relevant to either three or five successive points[108]). For three points the first derivative at the center (x_i) of the three points is

$$\dot{y}_i = \frac{1}{2h}(y_{i+1} + y_{i-1}) \qquad \text{(D3)}$$

except for the first and last points y_1 and y_n where the derivative is evaluated at the first and last points

$$\dot{y}_1 = \frac{1}{2h}(-3y_1 + 4y_2 - y_3)$$

$$\dot{y}_n = \frac{1}{2h}(3y_n - 4y_{n-1} + y_{n-2}) \quad . \tag{D4}$$

Likewise the five point Lagrange derivative reads for the third through third-from-last points

$$\dot{y}_i = \frac{1}{12h}\left[y_{i-2} - y_{i+2} + 8(y_{i+1} - y_{i-1})\right] \tag{D5}$$

with derivatives at the end points

$$\dot{y}_1 = \frac{1}{12h}\left[-25y_1 + 48y_2 - 36y_3 + 16y_4 - 3y_5\right]$$

$$\dot{y}_n = \frac{1}{12h}\left[25y_n - 48y_{n-1} + 36y_{n-2} - 16y_{n-3} + 3y_{n-4}\right] \tag{D6}$$

and adjacent to the end points

$$\dot{y}_2 = \frac{1}{12h}\left[-3y_1 - 10y_2 + 18y_3 - 6y_4 + y_5\right]$$

$$\dot{y}_{n-1} = \frac{1}{12h}\left[3y_n + 10y_{n-1} - 18y_{n-2} + 6y_{n-3} - y_{n-4}\right] \quad . \tag{D7}$$

In contrast to the seven point Stirling formula which computes the second derivatives directly, the Lagrangian formulae build the second derivatives by using the array of first derivatives as input. In this way a certain amount of "smoothing" is achieved.

Single and double precision routines for the above methods were used to compute second, fourth, sixth and eighth derivatives of sine curves for step sizes ranging from h = 0.05 to h = 0.30. The eighty input values for the sine curve with h = 0.05 covered less than a cycle while those with h = 0.30 covered almost four cycles.

Differences among the methods became quite apparent in the eighth derivatives with the five point double precision Lagrange method giving satisfactory accuracy (the sixth derivatives were usually accurate to one part in 10^4) for all eight derivatives over the entire range of step size. Least satisfactory was the method based upon Stirling's interpolating polynomial. It lost accuracy in the small step length - high derivative region. Roundoff error became troublesome in all cases in this small step length - high derivative region.

Despite these difficulties it was found that for the usual WBP model finite range corrections with a square well potential including second, fourth and sixth derivatives that all of these methods are of satisfactory accuracy. In this case computations of cross section, polarization and vector analyzing power with these different methods all agreed to within one percent.

LIST OF REFERENCES

1) S. T. Butler, Phys. Rev. 80 (1950) 1095.

2) S. T. Butler, Proc. Roy. Soc. A208 (1951) 559.

3) S. T. Butler, Phys. Rev. 88 (1952) 685.

4) S. T. Butler and O. H. Hittmair, Nuclear Stripping Reactions (John Wiley and Sons, Inc., New York, 1959).

5) J. Rotblat, Phys. Rev. 83 (1951) 1271.

6) J. Rotblat, Nature 167 (1951) 1027.

7) E. J. Burge, H. B. Burrows, W. M. Gibson and J. Rotblat, Proc. Roy. Soc. A210 (1951) 534.

8) A. Isoya and M. J. Marrone, Phys. Rev. 128 (1962) 800.

9) R. G. Allas and F. B. Shull, Phys. Rev. 116 (1959) 996.

10) A. Isoya, S. Micheletti and L. Reber, Phys. Rev. 128 (1962) 806.

11) A. S. Juveland and W. Jentsche, Phys. Rev. 110 (1958) 456.

12) L. H. Reber and J. X. Saladin, Phys. Rev. 133B (1964) 1155.

13) R. W. Bercaw and F. B. Shull, Phys. Rev. 133B (1964) 632.

14) W. P. Johnson and D. W. Miller, Phys. Rev. 124 (1961) 1190.

15) L. L. Lee, J. P. Schiffer, B. Zeidman, G. R. Satchler, R. M. Drisko and R. H. Bassel, Phys. Rev. 138 (1965) AB6.

16) T. A. Belote, W. E. Dorenbusch and J. Rapaport, Nucl. Phys. A120 (1968) 401.

17) H. G. Leighton, G. Roy and D. P. Gurd, Nucl. Phys. A115 (1968) 108.

18) K. K. Seth, J. Picard and G. R. Satchler, Nucl. Phys. A140 (1970) 577.

19) S. A. Andersen, O. Hansen, R. Chapman and S. Hinds, Nucl. Phys. A120 (1968) 421.

20) B. L. Cohen and O. V. Chubinsky, Phys. Rev. 131 (1963) 2184.

21) H. W. Fulbright, J. A. Robbins, R. West, D. P. Saylor and J. W. Verba, Nucl. Phys. A94 (1967) 214.

22) C. E. Hollandsworth, F. O. Purser, J. R. Sawers, Jr. and R. L Walter, Phys. Rev. 150 (1966) 825.

23) E. W. Hamburger, Phys. Rev. 123 (1961) 619.

24) U. Schmidt-Rohr, R. Stock and P. Turek, Nucl. Phys. 53 (1964) 77.

25) A. M. Baxter, J. A. R. Griffith and S. Roman, Phys. Rev. Letters 20 (1968) 1114.

26) T. J. Yule and W. Haeberli, Phys. Rev. Letters 19 (1967) 756.

27) H. H. Cuno, G. Clausnitzer and R. Fleischmann, Nucl. Phys. A139 (1969) 657.

28) University of Birmingham Report No. 711 (1971).

29) Proceedings of the Third International Symposium on Polarization Phenomena in Nuclear Reactions, ed. H. H. Barschall and W. Haeberli (University of Wisconsin Press, 1970).

30) J. A. R. Griffith, M. Irshad, O. Karban, S. W. Oh and S. Roman, Nucl. Phys. A167 (1971) 87.

31) D. Hilscher, J. C. Davis and P. A. Quin, Nucl. Phys. A174 (1971) 417.

32) T. J. Yule and W. Haeberli, Nucl. Phys. A117 (1968) 1.

33) C. A. Pearson, J. C. Wilcott and L. C. McIntyre, Nucl. Phys. A125 (1969) 111.

34) K. H. Bhatt and J. B. McGrory, Phys. Rev. C3 (1971) 2293.

35) P. Federman and S. Pitel, Nucl. Phys. A155 (1970) 161.

36) D. R. Bes and R. A. Broglia, Phys. Rev. C3 (1971) 2349.

37) H. Chandra and M. L. Rustgi, Phys. Rev. C4 (1971) 406.

38) M. L. Rustgi, H. W. King, R. Raj, R. A. Nisley and M. H. Hull, Jr., Phys. Rev. C4 (1971) 854.

39) M. MacFarlane, Bull. Am. Phys. Soc. 16 (1971) 1168.

40) E. Halbert, Bull. Am. Phys. Soc. 16 (1971) 1168.

41) C. R. Bingham and M. L. Halbert, Phys. Rev. C2 (1970) 2297.

42) R. W. Bercaw and R. E. Warner, Phys. Rev. C2 (1970) 297.

43) J. M. Morton, W. G. Davis, W. McLatchie, W. Darcey and J. E. Kitching, Nucl. Phys. A161 (1971) 228.

44) J. Horowitz and A. M. L. Messiah, J. Phys. Radium 14 (1953) 695.

45) J. Horowitz and A. M. L. Messiah, J. Phys. Radium 14 (1953) 737.

46) W. Tobocman, Phys. Rev. 94 (1954) 1655.

47) W. Tobocman, Phys. Rev. 115 (1959) 98.

48) W. Tobocman and W. R. Gibbs, Phys. Rev. 126 (1962) 1076.

49) G. R. Satchler, Nucl. Phys. 55 (1964) 1.

50) R. C. Johnson and P. J. R. Soper, Phys. Rev. C1 (1970) 976.

51) J. D. Harvey and R. C. Johnson, Phys. Rev. C3 (1971) 636.

52) C. A. Pearson and M. Coz, Nucl. Phys. 82 (1966) 545.

53) C. A. Pearson and M. Coz, Ann. of Phys. 39 (1966) 199.

54) C. A. Pearson, J. M. Bang and L. Pocs, Ann. of Phys. 52 (1969) 33.

55) C. A. Pearson, J. M. Bang and L. Pocs, Phys. Rev. 179 (1969) 1082.

56) C. A. Pearson, J. C. Wilcott and L. C. McIntyre, Nucl. Phys. A125 (1969) 111.

57) C. A. Pearson and J. C. Wilcott, Phys. Rev. 181 (1969) 1477.

58) C. A. Pearson, D. Zissermann and J. M. CoVan, Nucl. Phys. A152 (1970) 449.

59) C. A. Pearson, J. M. CoVan, D. Zissermann, T. G. Miller, F. P. Gibson, R. Haglund, W. Morrison and G. Westley, Nucl. Phys. A191 (1972) 1.

60) C. A. Pearson, D. Rickel and D. Zissermann, Nucl. Phys. A148 (1970) 273.

61) C. A. Pearson and D. Zissermann, Nucl. Phys. A154 (1970) 23.

62) C. A. Pearson, J. M. CoVan and D. Zissermann, Phys. Letters 35B (1971) 461.

63) R. C. Johnson, Nucl. Phys. A90 (1966) 289.

64) R. C. Johnson and F. Santos, Phys. Rev. Letters 19 (1967) 364.

65) W. E. Frahn and R. H. Lemmer, Nuovo Cim. 5 (1957) 1564.

66) W. E. Frahn and R. H. Lemmer, Nuovo Cim. 6 (1957) 664.

67) P. J. Wyatt, J. G. Wills and A. E. S. Green, Phys. Rev. 119 (1960) 1031.

68) F. G. Perey and B. Buck, Nucl. Phys. 32 (1962) 353.

69) F. G. Perey, Direct Interactions and Nuclear Reaction Mechanisms, ed. by E. Clementel and C. Villi (Gordon and Breach, New York, 1963), p. 125.

70) F. G. Perey and D. S. Saxon, Phys. Letters 10 (1964) 107.

71) N. Austern, Phys. Rev. 137 (1965) B752.

72) W. E. Frahn, Nucl. Phys. 66 (1965) 358.

73) H. Fiedeldey, Nucl. Phys. 77 (1966) 149.

74) J. K. Dickens, F. G. Perey, and R. J. Silva, International Nuclear Physics Conference, Gatlinburg (1966) 99.

75) H. Schulz, J. Wiebicke and R. R. Reif, Nucl. Phys. A101 (1967) 577.

76) W. Ulrici and W. R. Hering, Nucl. Phys. A110 (1968) 281.

77) N. Austern, R. M. Drisko, E. C. Halbert and G. R. Satchler, Phys. Rev. 133B (1964) 3.

78) R. M. Drisko and G. R. Satchler, Phys. Letters 9 (1964) 342.

79) J. K. Dickens, R. M. Drisko, F. G. Perey and G. R. Satchler, Phys. Letters 15 (1965) 337.

80) W. R. Smith, Nucl. Phys. A130 (1969) 657.

81) W. R. Smith, Phys. Rev. Letters 23 (1969) 1045.

82) W. R. Smith, Nucl. Phys. A94 (1967) 550.

83) P. J. A. Buttle and L. J. B. Goldfarb, Proc. Phys. Soc. 83 (1964) 701.

84) Gy. Bencze and J. Zimanyi, Phys. Letters 9 (1964) 246.

85) M. L. Goldberger and K. M. Watson, Collision Theory (John Wiley and Sons, Inc., New York, 1963).

86) H. Feshbach, C. E. Porter and V. F. Weisskopf, Phys. Rev. 96 (1954) 448.

87) H. Feshbach, Ann. of Phys. 5 (1958) 357.

88) D. Zissermann and C. A. Pearson, Department of Physics, University of Alabama, Birmingham, Alabama, to be published.

89) I. J. McGee, Phys. Rev. 151 (1966) 772.

90) T. Hamada and I. D. Johnston, Nucl. Phys. 34 (1962) 382.

91) M. E. Rose, Elementary Theory of Angular Momentum (John Wiley and Sons, Inc., New York, 1957), p. 61.

92) L. Fox, The Numerical Solution of Two-point Boundary Problems in Ordinary Differential Equations (Pergamon Press, Ltd., Oxford, 1957).

93) W. A. Watson, T. Philipson and P. J. Oates, Numerical Analysis - the Mathematics of Computing (American Elsevier Publishing Co., Inc., New York, 1969), p. 123.

94) J. M. Blatt and J. D. Jackson, Phys. Rev. 26 (1949) 18.

95) L. Hulthen and M. Sugawara, Handbook of Physics 39 (Springer-Verlag, Berlin, 1957), p. 3.

96) L. Rosen, J. G. Beery, A. S. Goldhaber and E. H. Auerbach, Ann. of Phys. 34 (1965) 96.

97) F. D. Becchetti and G. W. Greenlees, Phys. Rev. 182 (1969) 1190.

98) L. S. Michelman, S. Fiarman, E. J. Ludwig and A. E. Robbins, Phys. Rev. 180 (1969) 1114.

99) H. H. Cuno, G. Clausnitzer and R. Fleischmann, Nucl. Phys. A139 (1969) 657.

100) U. Schmidt-Rohr, R. Stock and P. Turek, Nucl. Phys. 53 (1964) 77.

101) K. Seth, J. Picard and G. R. Satchler, Nucl. Phys. A140 (1970) 577.

102) D. Kocher and W. Haeberli, Nucl. Phys. A172 (1971) 652.

103) C. T. Kelley, Jr., W. E. Maddox and D. W. Miller, Phys. Rev. 1C (1970) 488.

104) J. L. Alty, L. L. Green, R. Huby, G. D. Jones, J. R. Mines and J. F. Sharpey-Schafer, Nucl. Phys. A97 (1967) 541.

105) S. Kato, N. Takahashi, M. Takeda, T. Yamazaki and S. Yasukawa, Nucl. Phys. 64 (1965) 241.

106) W. Morrison, G. Westley and C. A. Pearson, Union Carbide Corp., Bldg. 6025, P. O. Box X, Oak Ridge National Laboratory, Oak Ridge, Tennessee 37830, to be published.

107) Z. Kopal, Numerical Analysis (Chapman & Hall, Ltd., London, 1955), p. 42.

108) F. B. Hildebrand, Introduction to Numerical Analysis (McGraw-Hill, New York, 1956), p. 82.